1993

The Origin of Mount St. Helens Andesites

Diane R. Smith
Trinity University, dsmith@trinity.edu

W. P. Leeman

Repository Citation

Smith, D.R., & Leeman, W.P. (1993). The origin of mount St. Helens andesites. *Journal of Volcanology and Geothermal Research, 55*(3), 271-303. doi:10.1016/0377-0273(93)90042-P

The origin of Mount St. Helens andesites

Diane R. Smith[a] and William P. Leeman[b]

[a]*Geology Department, Trinity University, 715 Stadium Drive, San Antonio, TX 78212, USA*

[b]*Keith-Wiess Geological Laboratories, Rice University, Houston, TX 77251, USA*

ABSTRACT

Smith, D. R. and Leeman, W. P., 1993. The origin of Mount St. Helens andesites. *J. Volcanol. Geotherm. Res.,* 55: 271-303.

Mount St. Helens volcano has intermittently produced mainly dacitic products but occasionally erupted a more diverse suite of lavas including basalts and andesites. Petrogenetic relations between these magmas provide insight into the dynamics of the subjacent magma system. Mineralogical and geochemical features of representative lavas erupted during the past 2200 years can distinguish three basaltic and three andesitic variants. The mafic lavas include: (a) transitional, olivine + plagioclase basalts with low K_2O and incompatible trace-element abundances: (b) calc-alkaline, olivine + plagioclase ± clinopyroxene basalts enriched in K_2O, TiO_2, and incompatible trace elements: and (c) calc-alkaline, olivine + plagioclase basaltic andesites with incompatible trace-element contents transitional between the two basalt types. Intermediate lavas include (a) tholeiitic, two-pyroxene andesites, (b) calc-alkaline, plagioclase + two-pyroxenes ± olivine ± amphibole mafic andesites (56-59% wt.% SiO_2), and (c) calc-alkaline, plagioclase + two-pyroxenes + amphibole high-silica andesites (61-62 wt.% SiO_2).

Eruption of these magmatic variants within the same eruptive phase implies the existence of different petrogenetic lineages, and that the plumbing system is sufficiently complex to simultaneously isolate and preserve numerous magma batches. It is unlikely that any of the andesites (or dacites) are derived by fractional crystallization of the recognized basaltic variants. Formation of the andesites simply by contamination (or assimilation-fractional crystallization) of basaltic magma is also improbable. More plausibly, the andesites represent mixing between basaltic and dacitic end-member magmas, each of which may be somewhat heterogeneous or vary in composition with time. In this model, efficient mixing must occur in some parts of the magma plumbing system, while some conduits or storage reservoirs must be effectively isolated.

Introduction

The Cascade volcanic arc of the northwestern United States has long been attributed to subduction of the Juan de Fuca plate beneath the North American plate. The large Quaternary to Recent volcanic centers of the arc, including Mount St. Helens, are complex systems that have erupted a wide range of magma types. The details of the volcanic stratigraphy at Mount St. Helens have been well documented (Hoblitt et al., 1980; Mullineaux and Crandell, 1981) and provide a framework in which to address the temporal evolution of the volcano.

In this paper, we present the details of the petrology and geochemistry of the youngest Mount St. Helens basaltic and andesitic eruptive products. We focus our discussion on the origin of the andesites and their relationship to other coeval magma types erupted at Mount St. Helens. Our major objectives are to evaluate the relative importance of such processes as fractional crystallization, assimilation, and magma mixing in producing the andesitic magmas, and to elucidate the nature of the magma system as a whole.

Geologic setting and eruptive history of Mount St. Helens

The Pacific Northwest has been a zone of convergence between North America and oceanic plates of the Pacific basin throughout much of Cenozoic time (Atwater, 1970; Lipman et al., 1972). In southern Washington, the Quaternary Cascade arc lies 250-300 km east of the convergent margin (Sherrod and Smith, 1990). Crustal thickness has been estimated as approximately 40-46 km everywhere beneath the Cascade Range (Mooney and Weaver, 1989) and the dip of the subducted slab is relatively steep (> 45º) (Michaelson and Weaver, 1986; Weaver and Michaelson, 1985).

Guffanti and Weaver (1988) subdivided the Cascade volcanic arc into five segments (Fig. 1) based on the distribution and composition of rocks erupted from Cenozoic volcanic vents less than 5 Ma in age. Mount St. Helens is situated within Guffanti and Weaver's Segment 2 which extends from Mount Rainier to Mount Hood. This 150-km-wide zone of vents is broader but has lower vent density than does the Oregon Cascades segment immediately to the south (between Mount Hood and Mount Shasta). To the north, Quaternary volcanism is limited to the stratovolcanoes of Glacier Peak and Mount Baker. Segment 2 is also the most seismically active portion of the Cascade Range (Weaver, 1989). These features and limited basaltic volcanism north of this segment were suggested by Weaver (1989) to be the result of the presence of a major crustal block in the southern Washington Cascades. On the basis of magnetotelluric data, this crustal block has been designated as the southern Washington Cascades conductor (Stanley et al., 1987), the western edge of which is coincident with the St. Helens seismic zone (Weaver, 1989). Mount St. Helens lies where structural trends intersect the St. Helens seismic zone (Weaver and Smith,

1983) and where small dextral offset on the seismic zone favors local crustal extension (Weaver, 1989).

Subduction-related magmatism in the vicinity of Mount St. Helens (MSH) dates back to Oligocene/early Miocene times, and the volcano was built during the past 40,000 years upon an eroded terrane of gently folded and altered volcanic and plutonic rocks (Evarts et al., 1987). The eruptive history of MSH has been divided into four eruptive stages (Crandell et al., 1975; Hoblitt et al., 1980; Mullineaux and Crandell, 1981). The most recent, the Spirit Lake stage, is subdivided as summarized in Table 1. The volcano has erupted a wide variety of magma types, ranging from basalt to rhyodacite. Dacitic (to rhyodacitic) magmas were erupted during each eruptive period within the Spirit Lake stage, but andesites were produced only during the Castle Creek, Kalama and Goat Rocks periods (andesite was also erupted in the Cougar stage, ~ 21 to 18 ka ago). Basaltic lavas and tephras were erupted only during the Castle Creek sequence. Detailed petrogenetic studies have been reported by Smith and Leeman (1987) for MSH dacites, and by Leeman et al. (1990) for Recent-Pliocene volcanic rocks from an E-W transect across the southern Washington Cascades. A recent synthesis of data concerning the magma reservoir beneath MSH, new chemical data that record mixing of basalt and dacite during the last 500 years, and implications of these data for volcanic hazards were reported by Pallister et al. (1992).

Sampling and analytical methods

The samples described in this study were collected both prior to (1978-79) and following (1982) the 1980 eruptive activity that destroyed much of the north flank of the volcano (see Appendix 1 for sample locations). Samples of Castle Creek products include basaltic to andesitic lavas from the now obliterated north flank of the volcano and from the south flank. The so-called 'cave' basalt (Verhoogen, 1937; Greeley and Hyde, 1972) found on the southwest side of the volcano and one andesitic scoria tephra (layer "Bh", Mullineaux, 1986) are also included. Kalama eruptive products include andesitic flows located on the south side of the volcano (Mullineaux and Crandell, 1981) and one scoria tephra (layer "Xb", Mullineaux, 1986). The single andesite lava flow (located on the northwest side of the volcano) produced during the Goat Rocks period is included (Lawrence, 1941). Two samples of Kalama andesite (MSH-484-1 and MSH-486-1) and one of Goat Rocks andesite (MSH-260-1) were provided by W. Melson and C. Hopson.

Minerals in selected samples were analyzed with a 3-channel ETEC microprobe as discussed in Smith (1984). Bulk-rock analyses were obtained by inductively-coupled plasma spectrometry (Rice Univ.) for major elements and V, Cu, Be, Ba, Sr, Zr, and Zn; by X-ray fluorescence (Open Univ. and Edinburgh Univ.) for Rb, Sr, Ba, Zr, Nb, Y, Pb, V, Cr, Co, Ni, and Cu; and by neutron activation (Radiation Center,

Oregon State Univ. and NASA-JSC) for Sc, Cr, Co, Ni, Cs, Sr, Ba, Rb, Zn, Hf, Ta, Th, U, and the rare earth elements (REE). Analytical errors are typically ± 1-3% for major elements and ± 2-10% for trace elements, except for Cr and Ni for which errors may be as high as 15%. For elements determined by more than one method, either averages or results by the most accurate method are reported. Most of the Sr isotopic data used in this paper are from Leeman et al. (in prep.); the $^{87}Sr/^{86}Sr$ ratios cited are precise to within ± 0.00003 or better.

Classification of lavas

We have subdivided MSH basalts and andesites into six groups mainly on the basis of SiO_2 contents and FeO*/MgO ratios (Table 2 and Fig. 2). The basaltic lavas include three variants, I-B, II-B, and III-BA, all of which were erupted during the Castle Creek period. Group I-B includes samples of the 'cave' basalt (cf. Verhoogen, 1937), which straddles the boundary between tholeiitic and calc-alkaline suites using the criteria of Irvine and Baragar (1971). Group II-B comprises superposed lava flows from the north flank. II-B lavas fall in the tholeiitic field of Figure 2, but their high K_2O content (~1.3 wt.%) defines them as calc-alkaline according to Irvine and Baragar's (1971) scheme. These lavas are also richer in TiO_2 than are other MSH basaltic lavas (cf. Table 2). Group III-BA includes superposed lava flows located on the north flank and other flows found on the south flank. These lavas are basalts and basaltic andesites having SiO_2 contents between ~51 and 54 wt.%; they straddle the boundary between tholeiitic and calc-alkaline types in Figure 2, but all samples fit Irvine and Baragar's (1971) definition of calc-alkaline rocks. Two samples fall within Gill's (1981) field for basic andesites, but the compositional gap between these rocks and other MSH andesites and their geochemical and mineralogical similarity to other III-BA samples suggest that the two samples belong to Group III-BA.

Andesitic lavas fall into three groups designated as I-A, II-A, and TH-A. Group I-A includes lavas and scoria of Kalama and Castle Creek age with SiO_2 contents ranging from ~56 to 59 wt.%. Group II-A andesites include lavas of Goat Rocks, Castle Creek, and Kalama age with higher SiO_2 contents (~61-62 wt.%) compared to I-A lavas. Both I-A and II-A andesites are calc-alkaline; tholeiitic andesites (TH-A) include two samples of lava and scoria of Castle Creek age.

Although II-A andesites have SiO_2 contents (61-62 wt.%) that overlap with some MSH dacites erupted during pre-Spirit Lake eruptive stages and the current eruptive period, these rock types are petrographically distinct. The low-silica dacites have field and petrographic features similar to dacites with SiO_2 contents >63 wt.%, i.e., they are light-colored, pumiceous tephras with phenocrysts of plagioclase, unreacted hornblende, and orthopyroxene, with or without cummingtonite (Smith and

Leeman, 1987). In contrast, the II-A andesites form blocky, thick, dark-colored lava flows with phenocrysts of plagioclase, clinopyroxene, orthopyroxene, and resorbed hornblende.

Petrography and mineral chemistry

Table 2 includes modal mineral proportions for MSH mafic to intermediate eruptive products. Representative analyses of minerals and compositional ranges of plagioclases from selected samples of each basaltic and andesitic compositional group are given in Table 3.

Basalts and basaltic andesites

The mafic rocks contain 11-23 vol.% phenocrysts (defined here as >0.3 mm) of olivine and plagioclase embedded in cryptocrystalline, intergranular or subophitic groundmasses consisting of plagioclase, Fe-Ti oxides, augite, olivine, and sparse pools of brown glass. Trace phenocrysts (up to 0.5 mm) and/or microphenocrysts of augite are found in a few samples of type II-B and III-BA lavas. I-B lavas are slightly coarser than are II-B and III-BA lavas. Glomerocrysts of olivine and/or plagioclase are present in all mafic lavas.

The phenocryst assemblage is dominated by subhedral to euhedral plagioclase grains (up to 2-3 mm) with clear to partially resorbed cores. Most phenocrysts are normally zoned (cores $\leq An_{85}$, rims $\leq An_{72}$); oscillatory zoning is infrequent. Groundmass grains are variable in composition (typical range being ~15 mole% An); their compositions are similar to or slightly more sodic than phenocryst rim compositions.

Most olivine phenocrysts (up to l-2 mm) are normally zoned (cores $\leq Fo_{84}$, rims $\leq F_{82}$), but some are homogeneous in composition. Core compositions in II-B and III-BA lavas tend to be more magnesian than those in the I-B lava, with the exception of the III-BA sample DS-74, which also has the lowest bulk-rock Mg-number [= 100 X molar Mg/ (Mg + Fe^{2+})] of the analyzed mafic rocks. Groundmass and microphenocryst grain compositions are within the range defined by phenocryst rims or are more Fe-rich. Olivine in a plagioclase +olivine clot in one of the III-BA samples (DS-4) has an anomalous composition (Fo_{66-67}) compared to olivine phenocrysts in the rock (Fo_{78-84} cores, Fo_{71-79} rims); the clot is probably xenocrystic. Spinel inclusions are present in olivine phenocrysts in II-B and III-BA mafic lavas, but appear to be lacking in the more Fe-rich olivine phenocrysts in I-B rocks.

A few of the basaltic andesites have distinctive groundmass textures. For example, basaltic andesite sample DS-4 contains roundish to feathery patches that are glassier than the surrounding material. A thin

section of this lava reveals a small (2-3 mm) “blob” of glassy material that appears to be dacitic; the groundmass of this inclusion consists of light brown glass (vs. black in the host rock) that is similar in composition (~73 wt.% SiO_2) to glasses in MSH pumiceous dacites (Fig. 3). The "blob" is also distinctive in that it lacks olivine but contains the only orthopyroxene microphenocrysts found in any of the mafic rocks. Orthopyroxene and plagioclase within the light brown glass have compositions similar to those found in MSH andesites and dacites.

Andesites

The andesites contain between 12 and 40 vol.% phenocrysts of plagioclase + orthopyroxene + clinopyroxene ± olivine ± hornblende ± Fe-Ti oxides (these minerals also form microphenocrysts). Glomerocrysts composed of various proportions of those minerals are found in nearly all samples. Abundant brown glass and plagioclase microlites are in the groundmasses in all but two I-A lavas, whereas groundmasses in II-A or TH-A lavas consist of fine, anhedral patches of plagioclase and cryptocrystalline material. Other differences among the andesite types include the absence of olivine in TH-A and II-A lavas and the absence of amphibole (or pseudomorphs after amphibole) in the TH-A lava. One sample (L82-48) has banding that is due to variable degrees of groundmass crystallinity; the bands contain the same mineral assemblage (e.g., olivine rimmed by pyroxene and amphibole pseudomorphs are found in all bands) in approximately the same proportions.

As in the mafic rocks, plagioclase is the dominant phenocryst (up to 2-3 mm) and generally makes up 80-90% of all phenocrysts by volume. These crystals exhibit various textures, including clear phenocrysts and phenocrysts with "sieve" textures. Although "sieve" implies that the growing crystal engulfed melt during growth (e.g., Glazner, 1990), we use this term to describe cores that appear to have undergone resorption or partial dissolution; some, in fact, may have formed by inclusion of melt during crystallization. We note that plagioclase textures which Kawamoto (1992) described as "dusty" and "honeycomb" both occur in individual MSH andesite samples. In most andesites, clear phenocryst cores have generally lower anorthite contents (An_{51-65}) than do those in the mafic lavas, the exception being a relatively plagioclase-poor II-A andesite (DS-2) where core compositions range from An_{61} to An_{75}. Phenocrysts with "sieve" textures in DS-70 (type II-A) have core compositions as calcic as An_{75-85} and rims of ~An_{50} (note that Table 3 does not include compositions for sieve-texture plagioclases in andesites). Oscillatory and reverse zoning also occur and are more common in the andesites than in the mafic lavas. Rim and groundmass grain compositions range from An_{49} to An_{69} in DS-2 and from An_{39} to An_{58} in the other analyzed andesites.

Olivine phenocrysts (< 2 vol.%; up to 1-2 mm) are present in type I-A andesites, usually as subhedral phenocrysts surrounded by thin (10-100 microns) reaction rims of pyroxene; unrimmed grains have embayed margins. Olivine also occurs in glomerocrystic clusters with pyroxene ± plagioclase ± Fe-Ti oxides. Sample DS-2 contains strongly zoned and Mg-rich olivine phenocrysts (Fo_{85} cores and Fo_{71} rims); this range exceeds that (5-10 mole%) typical of olivine phenocrysts in the mafic lavas. After Roeder and Emslie (1970), olivine core compositions in DS-2 suggest a coexisting melt composition with Mg-number (62) significantly higher than that observed (46) for the bulk lava; rim compositions, however, are consistent with equilibrium with the host melt.

Modal pyroxene contents range from < 0.5 to ~5 vol.%. Subhedral to euhedral orthopyroxene phenocrysts (up to 1 mm) have small compositional ranges (< 4 mole%) and most are either homogeneous or normally zoned. Some phenocrysts in sample DS-2 show small Mg-enrichment towards the rims. Alumina contents are variable, but rarely exceed 1.8 wt.%. Subhedral to euhedral clinopyroxene phenocrysts (up to 1-2 mm) show small compositional variations (< 5 mole%) and, of the grains analyzed, about half showed Fe-enrichment towards the rims and the others, Mg-enrichments. Al_2O_3 contents are variable and range from 1.2 to 3.6 wt.%, except for phenocrysts in sample DS-2 in which Al_2O_3 ranges from 1.8 up to 4.5 wt.% and Cr_2O_3 ranges up to 0.6 wt.% (the highest Cr_2O_3 in grains with the highest alumina contents).

In I-A lavas, the previous existence of small amounts (< 1 vol.%) of amphibole is inferred from pseudomorphs (up to 1 mm) of very fine opaque material, some of which have distinct prismatic or hexagonal shapes. In II-A lavas, the amphibole (tschermakitic to magnesiohastingsitic hornblende; cf. Leake, 1978) is partially to completely converted to granular oxides and silicates.

Trace amounts of magnetite and ilmenite form anhedral phenocrysts, microphenocrysts, and inclusions within silicate grains. Microprobe analyses show a large range in composition for oxide grains in lavas (e.g., TiO_2 contents vary from ~4 to 22 wt.% in a single titanomagnetite grain in sample DS-70), whereas a smaller range is observed for oxides in scoria (e.g., TiO_2 contents vary from ~12 to 15 wt.% in titanomagnetites in sample SH-3).

Bulk-rock geochemistry

Major elements

Excluding the tholeiitic andesites (TH-A), Harker diagrams (Fig. 4) reveal linear and negative correlations between SiO_2 (49-70 wt.%) and FeO, MgO, MnO (not shown), and CaO; a weaker trend is observed between SiO_2 and TiO_2. No obvious relationship exists between between Al_2O_3 and SiO_2; fairly wide ranges in alumina content exist for the basaltic andesites, andesites, and dacites. A roughly positive correlation exists between Na_2O and SiO_2. K_2O and P_2O_5 contents differ among the three mafic lava groups; the andesites have intermediate (to overlapping) K_2O and P_2O_5 contents between the basalts/basaltic andesites and the dacites.

Mg-numbers for the basalts and basaltic andesites range from 48 to 57. Calc-alkaline andesites (types I-A and II-A) have Mg-numbers (46 to 56) similar to those for the basalts and basaltic andesites, even though their MgO contents are lower. The tholeiitic andesites are distinct in having the lowest MgO contents (1.0-2.2) and Mg-numbers (29) of all MSH mafic rocks. Most MSH dacites have higher Mg-numbers than the tholeiitic andesites (as is evident from the FeO*/MgO ratios in Fig. 2).

Eruptive products of the Castle Creek period include all of the mafic and intermediate rock groups described here, as well as dacites (Fig. 2). Rhyodacite was extruded during the succeeding Sugar Bowl eruptive period. Kalama period volcanic rocks include mafic and silicic (types I-A and II-A) andesites and dacites and the Goat Rocks eruptive products consist of dacites and a silicic andesite (type II-A) lava flow. It appears that during the past 2200 years, the compositional range of magma erupted during a given eruptive period has become more restricted towards dacite with time (cf. Pallister et al., 1992). The volume of mafic and intermediate rocks also appears to decrease with time from the Castle Creek to the Goat Rocks eruptive period, although quantitative estimates are not available. However, the volumes of Kalama-age Plinian dacitic eruptive products (up to 2 km^3) are greater than those produced during the Goat Rocks (0.5 km^3) and current (<0.5 km^3) eruptive periods (Carey et al., 1989; Criswell, 1989).

Trace elements

Basalts and basaltic andesites

I-B and II-B basalt types have similar contents of Cr, V, Co, Sc and Ni, but are readily distinguished by relatively higher abundances of incompatible trace elements (K_2O, Sr, Rb, Ba, Zr, Nb, Hf, Ta, Th and light

REE) in II-B lavas (Table 4; Figs. 5 and 6a). Light REE abundances are higher in II-B ($(La/Yb)_N$ = 5.9-6.8) compared to I-B lavas ($(La/Yb)_N$ ~2.5), whereas heavy REE abundances are similar (10-12 times chondrites) in the two basalt types (Fig. 6).

Compared to I-B and II-B lavas, the basaltic andesites (III-BA) have wider abundance ranges for LILE, HFSE, and light REE that overlap with or are intermediate between the ranges for I-B and II-B lavas (Figs. 5 and 6a). The basaltic andesites have slightly lower or similar HREE contents (7.7-10.7 X chondrites) and intermediate $(La/Yb)_N$ ratios (3.9-4.6) compared to the basalts (Fig. 6b). None of the basalts have significant europium anomalies whereas a few basaltic andesites have slight positive anomalies (Eu/Eu* = ~1.1-1.2, as interpolated from Sm and Tb data).

Primordial mantle-normalized incompatible trace-element patterns (cf. Leeman et al., 1990) are similar for all three mafic magma types; they are fairly smooth, convex upward patterns typical of ocean island basalts (OIB). Unlike typical arc magmas, they do not display relative depletions in Nb and Ta. These patterns are typical of most basaltic rocks from the southern Washington Cascades (Leeman et al., 1990) and from the central Oregon Cascades (e.g., Hughes and Taylor, 1986; Hughes, 1990). In various incompatible-element ratio-ratio diagrams (e.g., Ba/Zr vs. Ta/Zr; Fig. 7), MSH mafic rocks plot along "mantle arrays" defined by mid-ocean ridge basalts (MORB) and OIB and lack the characteristic enrichments in LILE seen in most subduction-related magmas.

Andesites and dacites

In general, it is difficult to distinguish the andesite types based on their trace-element abundances. Although types I-A and II-A calc-alkaline andesites have overlapping trace-element abundances, the tholeiitic andesites are distinctive in having relatively higher HREE, Hf, Zr, and lower Ni, Sr, and $(La/Yb)_N$ (Figs. 5 and 6). SiO_2 is negatively correlated with V, Co, Sc, Ni, and Cr (not shown) in the more evolved MSH lavas (Fig. 5). The andesites are compositionally intermediate between the basalts and dacites. For elements with similar abundances among all basalt types (e.g., V, Co, Sc, Ni, Fe, Mg, Ca, Ti), near-linear variations with SiO_2 (correlation coefficients ~0.9 or higher for well determined elements) are observed for the basalt-andesite-dacite suite. Where the mafic rocks are compositionally diverse with regards to a particular element (e.g., K_2O, Al_2O_3, P_2O_5, Rb, Ba, Th, Sr, Zr, Hf, Ta), the andesites likewise display relatively wide variations of the element with SiO_2. Although Rb, Ba, Th, and Cs abundances generally increase with SiO_2, some dacites have similar or even lower abundances than do more mafic rocks; the andesites have similar to slightly higher abundances of these elements compared to the mafic rocks (Fig. 5). Sr, Zr, and Hf abundances are wide-ranging and nearly overlapping for the basalts/basaltic

andesites, andesites, and dacites (Fig. 5). Incompatible element ratio diagrams (Fig. 7) show that the andesites are intermediate between the mafic rocks and the dacites. Europium anomalies are lacking or small (Eu/Eu*= ~0.8-1.2) andesites.

Isotopes

Sr, Nd, Pb, and O isotope variations among southern Washington Cascades volcanic rocks have been summarized by Leeman et al. (1990). Halliday et al. (1983) and Leeman et al. (in prep.) present more detailed isotopic studies of MSH. The MSH basalt-andesite-dacite suite has small but significant ranges in $^{87}Sr/^{86}Sr$ (0.70301-0.70394), $^{143}Nd/^{144}Nd$ (0.512872-0.513012), and $\delta^{18}O$ (+5.7 to +7.6). Sr-Nd isotopic ratios for the basalts and basaltic andesites are similar to those for oceanic island basalts, whereas the andesites and dacites plot within or slightly to the right of the so-called "mantle array". For the purposes of this paper we emphasize that $^{87}Sr/^{86}Sr$ is strongly correlated with SiO_2 (Fig. 9).

Petrogenesis of MSH magmas

The following discussion summarizes the character and possible origins of MSH dacitic and basaltic rocks. We then focus on petrogenetic models for the andesites.

Dacitic rocks

Smith and Leeman (1987) observed that MSH dacites commonly are depleted in many incompatible elements (HREE, Be, U, HFSE) compared to basalts and andesites erupted from the volcano. Thus, the dacites are unlikely to be related to the associated mafic or intermediate magmas via fractional crystallization. They can be modeled as partial melts of an amphibolite source (hydrated MORB or primitive arc basalt) containing a small proportion of sediment to account for relative enrichment of LILE (Ba, Rb, Th, Cs, Sr) in the source (e.g., Fig. 7). We proposed that the dacites represent melts of sub-arc crust in response to intrusion of hot basaltic magma. Similar models have been suggested for silicic magmas elsewhere in the Cascades (e.g., Medicine Lake - Condie and Hayslip, 1975; Lassen volcanic center - Bullen and Clynne, 1990), in other volcanic arcs (e.g., Usu volcano, Japan - Fujimaki, 1986; Taupo volcanic zone, New Zealand - Cole, 1981), and in some ophiolite complexes (e.g., Canyon Mountain Complex, Oregon - Gerlach et al., 1981). Alternatively, Drummond and Defant (1990) have suggested that where young (<20-30 Ma) oceanic crust is being subducted, high-alumina dacite can be generated directly by slab melting involving garnet-bearing restite. The main difference between our

model and that of Drummond and Defant (1990) is the depth of the mafic source for high-alumina dacitic magmas. From observations of seismicity and eruptive behavior during the current eruptive period (Scandone and Malone, 1985; Barker and Malone, 1991) and from experimental studies (Merzbacher and Eggler, 1984; Rutherford et al., 1985), it is clear that dacitic magma was supplied from a mid-crustal (7-11 km) chamber, but the depth of the original source of dacite melts remains a debatable point. However, there is little doubt that basaltic and dacitic magmas coexisted during eruptive activity beginning with the Castle Creek period (Table 1). Smith and Leeman (1987) and Pallister et al. (1992) noted xenocrystic olivine and clinopyroxene in Goat Rocks and Kalama dacitic tephras. Other evidence of mingling between mafic and felsic magmas is found in Kalama-age banded scoria that contains basaltic bands with olivine and 58% SiO_2 glass in an andesitic matrix with 66% SiO_2 glass (Pallister et al., 1992). Heliker (1984) interpreted gabbroic nodules in MSH dacite dome rocks as representing crystallization of basaltic magma at depth, rather than crystal cumulates from the current eruptive period dacite, and Pallister et al. (1991) interpreted gabbroic xenoliths in older dome rocks as being scavenged from an active mafic pluton (vs. Tertiary basement) underlying MSH. The dacites thus tapped or traversed a region that had recently contained mafic magma (Pallister et al., 1992).

Basaltic rocks

We define three distinct mafic magma types at MSH which have fairly wide ranges in trace-element abundances and ratios. In addition, Leeman et al. (1990) documented other alkalic and tholeiitic variants in the nearby Mt. Adams, Indian Heaven, and Simcoe eruptive centers. The somewhat evolved nature of MSH basaltic rocks (e.g., Mg-number <57, Ni < 110 ppm, Cr <200 ppm, Co <42 ppm) suggests that they have experienced fractionation of small amounts of olivine ± plagioclase ± clinopyroxene, and some of the basaltic andesites (e.g., sample DS-4) may have experienced small degrees of mixing with silicic magmas. Nevertheless, these basalt types cannot be related to any single parental magma in light of the large differences in incompatible element contents and ratios among them (Figs. 7 and 8). There is no systematic inverse relation between compatible and incompatible element contents; Mg, Ni, Co, Cr, and V contents overlap for all basaltic variants despite large differences in Sr, Ba, and other incompatible elements (Figs. 4 and 5).

The observation that the mafic lavas lie within the "mantle array" defined by MORB and OIB for some incompatible element ratios (cf. Fig. 7) suggests that the basaltic magmas may be generated via melting of a heterogeneous reservoir composed of MORB and OIB mantle sources. Leeman et al. (1990) further discussed this variable mantle source model for the petrogenesis of southern Washington Cascades basalts

in general and noted that it is consistent with the tectonic and geologic history of the Pacific Northwest margin. An important observation made in that study was that most southern Washington Cascade basalts, including all MSH mafic rocks, lack compositional features (LILE enrichment and HFSE depletion) generally attributed to a subduction component (i.e., fluids released by dehydrating subduction lithosphere, subducted sediments).

MSH andesite petrogenesis

We consider MSH andesites to be either derivative or hybrid magmas as they have few of the expected properties for direct mantle melts or partial melts of subducted altered oceanic crust (Gill, 1981). Specific hypotheses considered here include crystal fractionation of basaltic magmas (e.g., Gill, 1981; Brophy, 1990), assimilation of crust by mafic magmas accompanied by fractional crystallization (AFC) (e.g., Grove et al., 1982; DePaolo, 1981; Davidson et al., 1987; Patterson and Graham, 1988), and mixing of mafic with felsic magmas (e.g., Eichelberger, 1975; Grove et al., 1982; Hickey-Vargas et al., 1989).

The role of crystal fractionation at MSH

Fractional crystallization (FC) is probably responsible for some of the compositional variations within MSH rock types, as demonstrated for the dacites (Smith and Leeman, 1987) and as suggested above for the basalts. However, this process cannot account for generation of the andesites from any of the mafic magma types. Removal of any feasible mineral assemblages from basaltic magmas fails to reproduce the trace-element characteristics of MSH andesites (Figs. 6 and 8). The only way to generate the basalt-andesite trend in Figure 6b via FC is to involve an amphibole- or garnet-rich assemblage, but this cannot explain the variations in incompatible trace-element ratios illustrated in Figure 8. Even considering analytical errors, the observed differences in these ratios within the MSH basalt-andesite-dacite suite are too large to be attributed to effects of crystal fractionation.

Isotopic data also preclude a closed-system genetic relationship between MSH basalts and andesites. The andesites have elevated $^{87}Sr/^{86}Sr$ compared to the basalts (Fig. 9; Halliday et al., 1983; Leeman et al., in prep.), and their formation clearly involves addition of isotopically distinct material during open system magmatic processes. Recent studies of radioactive ($^{226}Ra/^{230}Th$) disequilibrium between minerals and groundmass or bulk-rock samples provide further evidence for open-system magmatic processes (Volpe and Hammond, 1991).

The role of assimilation at MSH

We quantitatively modeled assimilation-fractional crystallization (AFC) processes to investigate the possibility that this process generates andesitic liquids from basaltic parents. The assimilants considered include upper crust (Taylor and McLennan, 1985), Tyee sediments (cf. table 8, Smith and Leeman, 1987) and selected MSH dacites. These lithologies were chosen to reflect representative continent-derived sediment and, in the case of the dacites, solidified magmas (or re-melts thereof) which may be present in the MSH sub-volcanic complex. Distribution coefficients used in the calculations are given in Table 5, and representative models are shown in Figures 8 and 10. These results reveal the following:

(1) Regardless of assimilant composition, type II-B basalts are not suitable mafic end members. Their La and Ba (and other incompatible element) contents are too high and alkalis/LREE ratios too low to produce the compositional characteristics of MSH andesites via AFC.

(2) The other two mafic end members (I-B and III-BA) produce observed characteristics of some MSH calc-alkaline andesites and one of the tholeiitic andesites, but only if large (0.5 or higher) rates of assimilation vs. crystallization operate and if large amounts of material (20-40%) are assimilated. Grove et al. (1989) found that such large amounts of assimilation are inconsistent with thermal models for melting of crust due to crystallization of basalt at shallow crustal levels. If mafic magmas are emplaced at shallow levels, it is more likely they will heat and cause the surrounding crust to melt (and possibly mix with those liquids) rather than crystallize and simultaneously assimilate solid crustal material (Grove et al., 1989).

(3) The models that appear to fit the observed trends for andesites in Figure 8 predict $^{87}Sr/^{86}Sr$ ratios which are within the range observed for some calc-alkaline and sites, to predict Sr contents of those andesites (filled triangles, Fig. l0). It is possible to generate MSH calc-alkaline andesites by AFC only if the parental magma contains more Sr than observed in MSH basalts. One of the tholeiitic andesites (DS-73) cannot be generated by any reasonable AFC models; its K/La, Ba/La, and $^{87}Sr/^{86}Sr$ ratios are too high compared to the calculated values (Figs. 8 and 10).

The role of magma mixing at MSH

Petrographic evidence in some of the MSH andesites studied supports magma mixing. Mineral-melt disequilibrium is indicated by resorption of olivine and pyroxene jackets on olivine phenocrysts (cf.

Tsuchiyama, 1986) in the mafic andesites (type I-A), and by the occurrence of plagioclase resorption textures in most andesites. The presence of olivine with cores of Fo_{85} in type I-A andesite suggests precipitation from a more mafic magma prior to mixing with dacitic magma. The calcic cores in some "sieve" textured plagioclases also indicate an origin from basaltic magma. Reverse zoning observed in some pyroxene and plagioclase phenocrysts is consistent with magma mixing, but other processes (e.g., changing water pressure, decreasing load pressure) could also produce these features. The phenocrysts could have re-equilibrated after mixing, causing many to become normally zoned.

An important aspect of MSH calc-alkaline andesites is that virtually all elemental/isotopic ratios and major/trace-element abundances are intermediate between the basaltic and dacitic rocks. This relationship is consistent with some form of mixing of dacitic and basaltic magmas. Furthermore, strong linear correlations exist between SiO_2 and some major and trace elements (e.g., MgO, CaO, V, Co; cf. Figs. 4 and 5), and between strontium and oxygen isotopic ratios (Smith et al., 1983). For these components, the basaltic and dacitic end members are relatively uniform. The lack of strong linear correlations between SiO_2 and other major and trace elements (e.g., P_2O_5, Al_2O_3, Sr, Zr, Hf; cf. Figs. 4 and 5) does not necessarily rule out mixing as the scatter may be attributed to variable end-member compositions coupled with some fractional crystallization subsequent to mixing.

Although probably oversimplistic, binary mixing models were calculated to test whether mixing between MSH basaltic and dacitic magmas can account for the major- and trace-element compositions of the andesites, and to constrain end-member compositions and relative proportions necessary to generate the andesitic magmas. Table 6 shows the results of the most successful models. The best fits are obtained when andesites and dacites of the same eruptive period are used in a given model (e.g., models M-1 and M-11). However, because basalts were erupted only during Castle Creek time, it was necessary to use compositions of those lavas in modeling andesites of other eruptive periods. It is possible that mafic magmas present in the magma system at other times could have had compositions slightly different from those used in the models.

Rather than rely on elemental abundances, which are sensitive to crystal removal and/or accumulation, we instead used incompatible trace-element ratios to constrain proportions of end members in models M-1 and M-II. In model M-1, hybrid andesite could be generated by mixing equal proportions of type 11-B basalt and dacite. This result is very similar to that of Pallister et al. (1992) for Kalama period andesitic scoria. Pallister et al. (1992) found other Kalama andesites more difficult to model and noted that additional magma-mixing end members are probably required. Basaltic andesites (type III-BA) were not

used in their models and may represent the mafic end member for those problematic andesites. We find a good fit for Goat Rocks andesite (similar in composition to some Kalama andesites) when 14% basaltic andesite mixes with 86% dacite (model M-II).

$^{87}Sr/^{86}Sr$ data are available for both end members and the selected hybrid used in model M-III; we used the isotopic data to constrain the proportions of end members required to produce the hybrid andesite. As with incompatible-element ratios, the ratios will not be affected by crystal fractionation. The result shows that 23% type II-B basalt is required to mix with 77% dacite to generate the modeled andesite.

Strontium isotopic data are not available for the specific andesites modeled in models M-I and M-II. The mixing proportions determined in those models (via incompatible-element ratios) predict $^{87}Sr/^{86}Sr$ to be 0.70338 and 0.70354, similar to Sr isotopic ratios available for other MSH andesites (~0.7035). Figure 10 shows that mixing models generally produce closer fits to the andesites than do AFC models, particularly considering the combined Sr-$^{87}Sr/^{86}Sr$ systematics. Nevertheless, the distinction between AFC model 4 and the mixing models is so slight that we cannot completely rule out the role of AFC in producing some andesites. For example, the tholeiitic andesites are more difficult to reproduce by mixing than are the calc-alkaline andesites. Agreement between calculated and observed abundances in these rocks is generally poor regardless of which criteria are used to constrain end-member proportions, or which end-member compositions are selected. Our modeling results indicate that AFC is as plausible as mixing in generating tholeiitic andesite.

In the models for calc-alkaline andesites presented in Table 6, elemental abundances (and LILE ratios) commonly agree within analytical uncertainties for both calculated and observed hybrids. None of the models succeeds in matching all components, particularly FeO, MgO, CaO, Ta, Sc, Co, but such discrepancies may result from other factors. A likely cause for misfits for these elements is uncertainty in choice of end members, especially the basalts. For example, substitution of a type II-B basalt (e.g., DS-6) as the mafic end member in model M-II produces an equally satisfactory fit. On the other hand, such calculations indicate that type I-B transitional basalts cannot be parental to the calc-alkaline andesites unless the felsic end member differs greatly in composition from MSH dacites (cf. Fig. 10). Furthermore, the basalt compositions used in the models may have been modified somewhat (e.g., by FC) compared to slightly more primitive magmas actually involved in mixing. For example, a less fractionated parent magma to basalt DS-6, containing > 700 ppm Sr, would be a more suitable end member to produce andesites DS-79 or MSH 486-1 (cf. Fig. 10). Additional diversity of MSH andesites could result from the involvement of more than two end members during mixing. Also, MSH andesites

may not represent magmas "captured" at the point of mixing; minor post-mixing FC (and re-equilibration of phenocrysts) may have operated prior to eruption. Even with these complexities, Figure 8 shows that magma mixing most closely reproduces the observed variations among MSH andesites than do the other processes considered (FC, AFC).

The mixing models indicate that some andesites may contain relatively low proportions (< 25%; models M-II and M-III) of a mafic end member. In such cases, it is unclear how relatively homogeneous hybrid magmas are physically produced. Production of such liquids is favored by high proportions of mafic to silicic end members (Sakuyama and Koyaguchi, 1984; Kouchi and Sunagawa, 1985; Sparks and Marshall, 1986). Where the fraction of mafic magma is low (<50%), the mafic magma is dispersed as solid xenoliths or inclusions within the silicic magma. However, the likelihood of homogenization increases as the thermal contrast between the two mixing magmas decreases and the water content of the mafic magma increases (cf. Thompson and Dungan, 1985; Sparks and Marshall, 1986). Pre-eruptive temperatures (~850-920°C) and water contents (~4-5% wt.%) for MSH dacites are constrained from Fe-Ti oxide thermometry (Smith and Leeman, 1987) and experimental studies (Merzbacher and Eggler, 1984; Rutherford et al., 1985). Although temperatures and water contents for MSH basaltic magmas are not known, if they were fairly hydrous and cool (< 1100°C; cf. Sisson and Grove, 1991), the temperature and viscosity contrasts between MSH dacite and basalt magmas may have been sufficiently small to promote efficient mixing even at low mafic magma proportions (cf. fig. 11 in Sparks and Marshall, 1986). It is also possible that mixing occurred in more than one stage. As pointed out by Thompson and Dungan (1985), single- and multi-stage mixing may produce similar geochemical trends, particularly if the system is not greatly modified by FC or AFC. The end members used in our mixing models may be slightly hybridized themselves; some basaltic andesites may have mingled with small amounts of silicic magma (Fig. 3) , and there is petrographic evidence that some dacites are themselves contaminated products of more silicic magma (Smith and Leeman, 1987; Pallister et al., 1992).

The MSH magma system

Seismological and experimental studies of the MSH magmatic system (e.g., Barker and Malone, 1991; Pallister et al., 1992) suggest that the MSH magmatic system is characterized by a deep (7-11 km), cylindrical magma reservoir with a volume between 5 and 7 km^3 which vents magma to the surface through a narrow conduit system (Scandone and Malone, 1985). A northeast-striking fault at depths > 11 km may be a conduit to transport (basaltic?) magma from greater depths within the crust to the reservoir at 7-11 km depth (Barker and Malone, 1991). Dacite eruptions from 1980 to the present appear to have

vented the upper levels of the reservoir-conduit system (e.g., Rutherford et al., 1985; Carey et al., 1990; Pallister et al., 1992).

The petrology and geochemistry of MSH eruptive products seemingly require additional complexity in the sub-volcanic plumbing system as sampled during Castle Creek time when a wide variety of magma types, ranging from basalt to dacite, were erupted (Table 1). For example, the 'cave' basalt (type I-B) is believed to have erupted along the south flank at about the same time as other basaltic lava types (types II-B and III-BA) vented on the north side of the volcano (Crandell, 1987). Although slightly fractionated, these magma types are chemically distinct and not easily related to one another through evolutionary processes nor by melting of a common mantle source. Castle Creek eruptions also included dacites (interpreted as variably evolved crustal melts) and a suite of compositionally diverse hybrid andesites. Kalama period is also characterized by a variety of andesitic and dacitic eruptive products (Table 1), but the existence of basaltic magmas within the system during this time is inferred on the basis of petrographic observations and geochemical models presented here and by Pallister et al. (1992). Eruptive products of the Goat Rocks period are more restricted in composition (type II-A andesite and dacite), but the presence of more mafic magmas during that interval is implied by petrological and geochemical evidence for mixing in those eruptive products.

These observations suggest important implications concerning the nature of the MSH magma system. Because nearly the entire spectrum of magma types observed at MSH was produced during the Castle Creek period, it is clear that each variant was available during this time. Also, although eruptive products were less diverse during the other eruptive periods, evidence for hybridization in some magmas produced subsequent to the Castle Creek period attests to the persistent complexity of the plumbing system. To explain the petrologic evolution and eruptive history of MSH, we infer that the plumbing system repeatedly has accommodated isolated storage of relatively primitive mafic magmas and anatectic dacitic magmas. Hybridized intermediate composition magmas, attributed to mixing between these extreme magma types or between other hybrid end members, also must have been stored locally within the system. We envision a complex plumbing system with multiple conduits, some of which tap mafic and felsic reservoirs and allow mixing between these magmas, and others which tap effectively isolated reservoirs. Apparently, efficient mixing occurred in some parts of the plumbing system and not in others. Several interesting configurations are suggested. For example, if basaltic magmas melt the crust to form dacite, then subsequent mixing of ascending basalt with anatectic melt may form some andesites. Another scenario involves stagnation of primitive, denser basalt deep in the crust, whereas more evolved, less dense basaltic differentiates may ascend to shallower levels, creating a stratified system. Further

stratification may result from emplacement of dacites above the mafic differentiates. Magma mixing resulting in homogeneous hybrids requires the breakdown of this stratification, perhaps by high-velocity injection of turbulent plumes of primitive magma into the base of the chamber (Sparks et al., 1980; Sakuyama and Koyaguchi, 1984), forced convection during flow in sub-volcanic conduits (Kouchi and Sunagawa, 1985; Koyaguchi, 1985), or convective turbulence generated by large differences in temperature between end members (Nixon, 1988).

Conclusions

Several lines of evidence suggest that mafic magmas have been more important at MSH than commonly realized, particularly considering the persistent eruption of dacitic magmas over the past 36 ka. True basaltic lavas were produced only during the Castle Creek eruptive period (1.7-2.2 ka) at which time at least three compositionally distinct variants issued forth. It is probably not coincidental that this period marked the appearance of the first significant outpourings of intermediate composition lavas (three variants of andesite). Andesites were produced intermittently during the subsequent eruptive episodes (as recently as 1857 A.D.).

The petrographic and geochemical data presented here are inconsistent with simple cogenetic relationships among these diverse magmas. Although all magmas underwent varied degrees of fractional crystallization and some perhaps assimilated small amounts of wall rocks, the broad compositional spectrum represented by MSH magmas cannot be explained as the result of these processes alone. The extreme basaltic and dacitic magma types plausibly represent partial melts of distinct mantle and crustal sources, respectively. Crustal melting to produce the dacites was likely triggered by emplacement of ascending basaltic magmas within the sub-arc crust (Smith and Leeman, 1987). It is proposed here that most of the intermediate composition magmas essentially formed as products of single- or multi-stage mixing between mafic and dacitic magmas (sensu latu). Thus, in our view, all MSH magmatism has been driven by basaltic magmatism.

The diversity of magma types erupted during Castle Creek time implies a complex sub-volcanic plumbing system that allows for the coexistence of several end-member and hybrid magma types. Evidently, compartmentalization allows segregation of diverse magma batches, yet periodic communication between different parts of the system results in efficient mixing to produce hybrid magmas. Temporal trends suggest a decreasing role for a basaltic component in magmas erupted from the volcano from ~2200 years to the present; this may reflect diminishing influx of basaltic magmas or selective tapping of shallower parts of the system with time.

Acknowledgements

This research was supported by the National Science Foundation (grants EAR 79-19998, EAR 82-14876, EAR 85-12172, and EAR 90-14802). DRS acknowledges additional support from the Penrose Foundation and Trinity University. We thank R. Schmitt (Oregon State University) and D. Blanchard (NASA-JSC) for access to neutron activation facilities, and J. Watson (Open University) for access to X-ray fluorescence facilities. We are grateful to M. Norman and G. Fitton for providing INAA and XRF analyses, C. Hopson for a copy of his geologic map of MSH, R. Hermens for field assistance, and W. Melson and C. Hopson for providing three samples. Thorough and constructive reviews by J. Pallister and D. Draper greatly contributed to the quality of the manuscript.

Appendix I

Appendix 1

Sample location descriptions. Map units Qsa_2, Qsa_3, etc. are from Hopson (unpub. map, 1977).

Sample(s)	Location
DS-61	SW 1/4, NW 1/4, Sect. 12, T. 8 N., R. 5 E., ~1245' elev.; andesite lava (Qsa_2) taken at head of Ape Canyon
DS-73; DS-71; DS-72; DS-74; DS-76; DS-77; DS-78	SE 1/4 SW 1/4, Sect. 28, T. 9 N., R. 5 E.; basaltic to andesitic lavas occurring in a stream valley on north flank of volcano (cf. Figure 11 in Verhoogen, 1937). Lavas were collected along east and west valley walls. Samples taken from west wall from bottom to top of flow pile include: DS-73, DS-71 (~1385' elev.), DS-72. Samples taken from east wall from bottom to top of flow pile include: DS-74, DS-76, DS-77, DS-78 (~1400'elev.).
DS-70	SE 1/4, SW 1/4, Sect. 29, T. 9 N., R. 5 E.; north-northwest or "floating island" lava flow of Lawrence (1941); andesite lava (Qsa_2)
DS-79	NE 1/4, NW 1/4, Sect. 20, T. 8 N., R. 5 E., ~1350' elev.; south-southwest andesite flow (Qsa_2) near Butte camp
DS-27	SE 1/4, SE 1/4, Sect. 25, T. 7 N., R. 4 E.; Cave basalt flow (Verhoogen, 1937; Greeley and Hyde, 1972) occurring on the north side of National Forest Road 90; 4.8 km west of Cougar on N90
DS-33	SW 1/4, NE 1/4, Sect. 23, T. 8 N., R. 5 E.; andesite flow (Qsa_2); lava pile at end of road N826, ~0.4 km in from road
SH-3	NE 1/4, SW 1/4, Sect. 26, T. 9 N., R. 5 E.; "Xb" andesite tephra (Mullineaux, 1986)
SH-25	SE 1/4, SE 1/4, Sect. 19, T. 9 N., R. 6 E.; "Bh" andesite tephra (Mullineaux, 1986)
DS-4; DS-5; DS-6; DS-7; DS-9; DS-2	SE1/4, NW 1/4, Sect. 34, T. 9 N., R. 5 E. (approximately equivalent to Location 4, Plate in Crandell, 1987); basalt and andesite lava flows occurring on north flank of volcano sampled sequentially from top to bottom of flow pile include: DS-4 (~1465' elev.), DS-5 (~1450' elev.), DS-6 (between 1430 and 1465' elev.), DS-7 (~1430' elev.); DS-9, DS-2 (~1410' elev)
L82-57	SE 1/4, SW 1/4, Sect. 18, T. 8 N., R. 5 E.; south-southwest andesite flow (Qsa_3), north of Butte Camp
L82-47	SW 1/4, NE 1/4, Sect. 22, T. 8 N., R. 5 E., ~1340' elev.; andesite flow (Qsa_2)
L82-45	NW 1/4, SE 1/4, Sect. 22, T. 8 N., R. 5 E., ~1220' elev.; andesite flow (Qsa_2)
L82-44	SW 1/4, SE 1/4, Sect. 22, T. 8 N., R. 5 E., ~1150' elev.; andesite flow (Qsa_2)
L82-48	NE 1/4, NW 1/4, Sect. 27, T. 8 N., R. 5 E., ~1145' elev.; andesite flow (Qsa_2)
L82-42	NW 1/4, SE 1/4, Sect. 27, T. 8 N., R. 5 E., ~975' elev.; massive andesite (Qsa_6) in place in East fork of Swift Creek
L82-40; L82-41A	SW 1/4, SW 1/4, Sect. 28, T. 8 N., R. 5 E.; basalt flow (Qsb_1)
L82-55	SE 1/4, SW 1/4, Sect. 29, T. 8 N., R. 5 E.; basalt flow (Qsb_1)
L82-56	NW 1/4, NW 1/4, Sect. 32, T. 8 N., R. 5 E.; basalt flow (Qcb_1)
L82-63	SE 1/4, NW 1/4, Sect. 33, T. 8 N., R. 5 E.; basalt flow (Qcb_1), along road 0.5 km south of Jct. 81 and Kalama workcenter road
L82-59	Junction of 82 with Rd. 8123 west of McBride Lake; andesite flow ($Qsag_2$)
SH-21	SW 1/4, SW 1/4, Sect. 20, T. 9 N., R. 6 E.; "Pm" dacite tephra (Mullineaux, 1986)
SH-18	SE 1/4, NW 1/4, Sect. 15, T. 8 N., R. 6 E.; "We" dacite tephra (Mullineaux, 1986)
DS-41	SW 1/4, NW 1/4, Sect. 24, T. 9 N., R. 5 E.; "T" dacite tephra (Mullineaux, 1986)

References

Atwater, T., 1970. Implications of plate tectonics for the Cenozoic tectonic evolution of western North America. Geol. Soc. Am. Bull., 81: 3513-3536.

Barker, S.E. and Malone, S.D., 1991. Magmatic system geometry at Mount St. Helens modeled from the stress field associated with posteruptive earthquakes. J. Geophys. Res., 96: 11,883-11,894.

Brophy, J.G., 1990. Andesites from northeastern Kanaga Island, Aleutians. Contrib. Mineral. Petrol., 104: 568-581.

Bullen, T.D. and Clynne, M.A., 1990. Trace element and isotopic constraints on magmatic evolution at Lassen volcanic center. J. Geophys. Res., 95: 19,671-19,691.

Carey, S., Gardner, J. and Sigurdsson, H., 1989. Intensity and magnitude of post-glacial Plinian eruptions at Mount St. Helens. In: Abstracts, lAVCEI General Assembly on Continental Magmatism. N.M. Bur. Mines Miner. Resour. Bull., 131: 43.

Carey, S., Sigurdsson H., Gardner, J.E. and Criswell, W., 1990. Variations in column height and magma discharge during the May 18, 1980 eruption of Mount St. Helens. J. Volcanol. Geotherm. Res., 43: 99-112.

Cole, J.W., 1981. Genesis of lavas of the Taupo volcanic zone, North Island, New Zealand. J. Volcanol. Geotherm. Res., 10: 317-337.

Condie, K.D. and Hayslip, D.L., 1975. Young bimodal volcanism at Medicine Lake volcanic center, northern California. Geochim. Cosmochim. Acta, 39: 1165-1178.

Crandell, D.R., 1987. Deposits of pre-1980 pyroclastic flows and lahars from Mount St. Helens volcano, Washington. U.S. Geol. Surv., Prof. Pap. 1444, 91 pp.

Crandell, D.R., Mullineaux, D.R. and Rubin, M.. 1975. Mount St. Helens volcano: Recent and future behavior. Science. 187: 438-441.

Criswell, W., 1989. Volumes and compositional variations of the May 18, 1980 eruption of Mount St. Helens: implications for eruption forecasts. In: Abstracts, lAVCEI General Assembly on Continental Magmatism. N.M. Bur. Mines Miner. Resour. Bull., 131: 62.

Davidson, J.P., Dungan, M.A., Ferguson, K.M. and Colucci, M.T., 1987. Crust-magma interactions and the evolution of arc magmas: the San Pedro-Pellado volcanic complex, southern Chilean Andes. Geology, 15: 443-446.

DePaolo, D.J., 1981. Trace element and isotopic effects of combined wallrock assimilation and fractional crystallization. Earth Planet. Sci. Lett., 53: 189-202.

Dostal, J., Dupuy, C., Carron, J.P., LeGuen de Kerneizon, M. and Maury, R.C., 1983. Partition coefficients of trace elements; application to volcanic rocks of St. Vincent, West Indies. Geochim. Cosmochim. Acta, 47: 525-533.

Drummond, M.S. and Defant, M.J., 1990. A model for trondhjemite-tonalite-dacite genesis and crustal growth via slab melting: Archean to modern comparisons. J. Geophys. Res., 95: 21,503-21,521.

Eichelberger, J.C., 1975. Origin of andesite and dacite: evidence of mixing at Glass Mountain in California and at other Circum-Pacific volcanoes. Geol. Soc. Am. Bull., 86: 1381-1391.

Evarts, R.C., Ashley, R.P. and Smith, J.G., 1987. Geology of the Mount St. Helens area: record of discontinuous volcanic and plutonic activity in the Cascade Arc of southern Washington. J. Geophys. Res., 92: 10,155-10,169.

Fujimaki, H., 1986. Fractional crystallization of the basaltic suite of Usu volcano, southwest Hokkaido, Japan and its relationships with the associated felsic suite. Lithos, 19: 129-140.

Gerlach, D.C., Leeman, W.P. and Ave Lallemant, H.G., 1981. Petrology and geochemistry of plagiogranite in the Canyon Mountain Ophiolite, Oregon. Contrib. Mineral. Petrol., 77: 82-92.

Gill, J.B., 1981. Orogenic Andesites and Plate Tectonics. Springer-Verlag, New York, NY, 290 pp.

Glazner, A., 1990. Recycling of continental crust in Miocene volcanic rocks from the Mojave block, southern California. Geol. Soc. Am. Mem., 174: 147-168.

Greeley, R. and Hyde, J.H., 1972. Lava tubes of the Cave Basalt. Geol. Soc. Am. Bull., 83: 2397-2418.

Grove, T.L., Gerlach, D.C. and Sando, T.W., 1982. Origin of calc-alkaline series lavas at Medicine Lake volcano by fractionation, assimilation and mixing. Contrib. Mineral. Petrol., 80: 160-182.

Grove, T.L., Baker, M.B., Kinzler. R.J. and Donnelly-Nolan, J.M., 1989. Evidence for the generation of calc-alkaline andesites from compositionally zoned lava at Medicine Lake Volcano, N. California. In: Abstracts, IAVCEI General Assembly on Continental Magmatism. N.M. Bur. Mines Miner. Resour. Bull., 131: 115.

Guffanti, M. and Weaver, C.S.. 1988. Distribution of Late Cenozoic volcanic vents in the Cascade Range: volcanic arc segmentation and regional tectonic considerations. J. Geophys. Res., 93: 6513-6529.

Halliday, A.N., Fallick, A.E., Dickin, A.P., Mackenzie, A.B., Stephens, W.E. and Hildreth, W., 1983. The isotopic and chemical evolution of Mount St. Helens. Earth Planet. Sci. Lett., 63: 241-256.

Heliker, C., 1984. Inclusions in the 1980-83 dacite of Mount St. Helens, Washington. Master's thesis. Western Washington University, 185 pp.

Henderson, P., 1982. Inorganic Geochemistry. Pergamon Press, Oxford, England, 353 pp.

Hickey-Vargas, R., Roa, H.M., Escobar, L.L. and Frey, F.A., 1989. Chemical variations in Andean basaltic and silicic lavas from the Villarrica-Lanin volcanic chain (39.5°S): evaluation of source heterogeneity, fractional crystallization and crustal assimilation. Contrib. Mineral. Petrol., 103: 361-386.

Hoblitt, R.P., 1989. Day 3: The Kalama eruptive period, southwest and south flanks. In: C.E. Chapin and J. Zidek (Editors), Field Excursions to Volcanic Terranes in the Western United States. Volume II: Cascades and Intermountain West. N.M. Bur. Mines Miner. Resour. Mem., 47: 65-69.

Hoblitt, R.P., Crandell, D.R. and Mullineaux, D.R., 1980. Mount St. Helens eruptive behavior during the last 1500 years. Geology, 8: 555-559.

Hole, M.J., Saunders, A.D., Marriner, G.F. and Tarney, J., 1984. Subduction of pelagic sediments: implications for the origin of Ce-anomalous basalts from the Mariana Islands. J. Geol. Soc. London, 14:453-472.

Honjo, N. and Leeman, W.P., 1987. Origin of hybrid ferrolatite lavas from Magic Reservoir eruptive center. Snake River Plain, Idaho. Contrib. Mineral. Petrol., 96:163-177.

Hughes, S.S., 1990. Mafic magmatism and associated tectonism of the central High Cascade Range, Oregon. J. Geophys. Res., 95: 19,623-19,638.

Hughes, S.S. and Taylor, E.M., 1986. Geochemistry, petrogenesis, and tectonic implications of central High Cascade mafic platform lavas. Geol. Soc. Am. Bull., 97: 1024-1036.

Irvine, T.N. and Baragar, W.R., 1971. A guide to the chemical classification of the common igneous rocks. Can. J. Earth Sci., 8: 523-548.

Kawamoto, T., 1992. Dusty and honeycomb plagioclase: indicators of processes in the Uchino stratified magma chamber, Izu Peninsula, Japan. J. Volcanol. Geotherm. Res., 49: 191-208.

Koyaguchi, A., 1985. Magma mixing in a conduit. J. Volcanol. Geotherm. Res., 25: 365-369.

Kouchi, A. and Sunagawa, I., 1985. A model for mixing basaltic and dacite magmas as deduced from experimental data. Contrib. Mineral. Petrol., 89: 17-23.

Lawrence, D.B., 1941. The "floating island" lava flow of Mt. St. Helens. Mazama, 23: 56-60.

Leake, B.E., 1978. Nomenclature of amphiboles. Am. Mineral., 65: 1023-1052.

Leeman, W.P., Smith, D.R., Hildreth, W., Palacz, Z. and Rogers, N., 1990. Compositional diversity of Late Cenozoic basalts in a transect across the southern Washington Cascades: implications for subduction zone magmatism. J. Geophys. Res., 95: 19,561-19,582.

Lipman, W., Prostka, B.J. and Christiansen, R.L., 1972. Cenozoic volcanism and plate-tectonic evolution of the United States: I. Early and Middle Cenozoic. Philos. Trans. R. Soc. London, Ser. A, 271: 217-248.

Merzbacher, C.L. and Eggler, D.H., 1984. A magmatic geohygrometer: application to Mount St. Helens and other dacitic magmas. Geology, 12: 587-590.

Michaelson, C.A. and Weaver, C.S., 1986. Upper mantle structure from teleseismic P wave arrivals in Washington and northern Oregon. J. Geophys. Res., 91: 2077-2094.

Miyashiro, A., 1974. Volcanic rock series in island arcs and active continental margins. Am. J. Sci., 274: 321-355.

Mooney, W.D. and Weaver, C.S., 1989. Regional crustal structure and tectonics of the Pacific coastal states; California, Oregon, and Washington. Geol. Soc. Am. Mem., 172: 129-161.

Mullineaux, D.R. and Crandell, D.R., 1981. The eruptive history of Mount St. Helens. U.S. Geol. Surv., Prof. Pap., 1250: 3-15.

Mullineaux, D.R., 1986. Summary of pre-1980 tephra-fall deposits erupted from Mount St. Helens, Washington State, USA. Bull. Volcanol., 48: 17-26.

Nixon, G.T., 1988. Petrology of the Younger Andesites and Dacites of Iztaccihuatl volcano, Mexico: I. Disequilibrium phenocryst assemblages as indicators of magma chamber processes. J. Petrol., 29: 213-264.

Pallister, J.S., Heliker, C. and Hoblitt, R.P., 1991. Glimpses of the active pluton below Mount St. Helens. EOS, Trans. Am. Geophys. Union, 72: 576.

Pallister, J.S., Hoblitt, R.P., Crandell, D.R. and Mullineaux, D.R., 1992. Mount St. Helens a decade after the 1980 eruptions: magmatic models, chemical cycles, and a revised hazards assessment. Bull. Volcanol., 54:126-146.

Patterson, D.S. and Graham, I.J., 1988. Petrogenesis of andesitic lavas from Mangatepopo Valley and Upper Tama Lake, Tongariro volcanic centre, New Zealand. J. Volcanol. Geotherm. Res., 35: 17-29.

Pearce, J.A. and Norry, M.J., 1979. Petrogenetic implications of Ti, Zr, Y and Nb variations in volcanic rocks. Contrib. Mineral. Petrol., 69: 33-47.

Riddihough, R., 1984. Recent movements of the Juan de Fuca plate system. J. Geophys. Res., 89: 6980-6994. Roeder, P.L. and Emslie, R.F., 1970. Olivine-liquid equilibrium. Contrib. Mineral. Petrol., 29: 275-289.

Rutherford, M.J., Sigurdsson, H., Carey, S. and Davis, A., 1985. The May 18, 1980, eruption of Mount St. Helens: I. melt composition and experimental phase equilibria. J. Geophys. Res., 90: 2929-2947.

Sakuyama, M. and Koyachugi, T., 1984. Magma mixing in mantle xenolith-bearing calc-alkalic ejecta, Ichinomegata volcano, northeastern Japan. J. Volcanol. Geotherm. Res., 22: 199-224.

Scandone, R. and Malone, S.D., 1985. Magma supply, magma discharge and readjustment of the feeding system of Mount St. Helens during 1980. J. Volcanol. Geotherm. Res., 23: 239-262.

Sherrod, D.R. and Smith, J.G., 1990. Quaternary extrusion rates of the Cascade Range, northwestern United States and southern British Columbia. J. Geophys. Res., 95(B12): 19,465-19,474.

Shimizu, N. and Kushiro, I., 1975. The partitioning of rare earth elements between garnet and liquid at high pressure: preliminary experiments. Geophys. Res. Lett., 2: 413-416.

Sisson, T.W. and Grove, T.L., 1991. Estimating the water content of aluminous arc magmas. EOS, Trans. Am. Geophys. Union, 72: 292.

Smith, D.R., 1984. The petrology and geochemistry of High Cascade volcanics in southern Washington: Mount St. Helens volcano and the Indian Heaven basalt field. Ph.D. thesis, Rice University, 409 pp.

Smith, D.R. and Leeman, W.P., 1987. Petrogenesis of Mount St. Helens dacitic magmas. J. Geophys. Res., 92: 10,313-10,334.

Smith, D.R., Matsuhisa, Y., Kurasawa, H. and Leeman, W.P., 1983. Oxygen and strontium isotopic variations in Mount St. Helens eruptive products. EOS, Trans. Am. Geophys. Union, 64: 894.

Sparks, R.S.J. and Marshall, L.A., 1986. Thermal and mechanical constraints on mixing between mafic and silicic magmas. J. Volcanol. Geotherm. Res., 29:99-124.

Sparks, R.S.J., Meyer: and Sigurdsson, H., 1980. Density variation amongst mid-ocean ridge basalts: implications for magma mixing and the scarcity of primitive lavas. Earth Planet. Sci. Lett., 46: 419-430.

Stanley, W.D., Finn, C. and Plesha, J.L., 1987. Tectonics and conductivity structures in the southern Washington Cascades. J. Geophys. Res., 92: 10,179-10,193.

Taylor, S.R. and McLennan, S.M., 1985. The Continental Crust: Its Composition and Evolution. Blackwell Scientific Publications, Oxford, England, 312 pp.

Thompson, R.A. and Dungan, M.A., 1985. The petrology and geochemistry of the Handkerchief Mesa magma complex, San Juan Mountains, Colorado. J. Volcanol. Geotherm. Res., 26: 251-274.

Tsuchiyama, A., 1986. Experimental study of olivine-melt reaction and its petrological implications. J. Volcanol. Geotherm. Res., 29: 245-264.

Verhoogen, J., 1937. Mount St. Helens -- a recent Cascade volcano. Calif. Univ. Dep. Geol. Sci. Bull., 24(9): 263-302.

Volpe, A.M. and Hammond, E., 1991. ^{238}U-^{230}Th-^{226}Ra disequilibria in young Mount St. Helens rocks: time constraint for magma formation and crystallization. Earth Planet. Sci. Lett., 107:475-486.

Weaver, C.S., 1989. Seismicity of the Cascade Range and adjacent areas. In: L.J. Muffler, C.S. Weaver and D.D. Blackwell (Editors), Geological, Geophysical, and Tectonic Setting of the Cascade Range. U.S. Geol. Surv., Open-File Rep., 89-178: 74-93.

Weaver, C.S. and Baker, G.E., 1988. Geometry of the Juan de Fuca plate beneath Washington -- evidence from seismicity and the 1949 South Puget Sound earthquake. Bull. Seismol. Soc. Am., 78: 264-275.

Weaver, C.S. and Michaelson, C.A., 1985. Seismicity and volcanism in the Pacific Northwest: evidence for the segmentation of the Juan de Fuca plate. Geophys. Res. Lett., 12: 215-218.

Weaver, C.S. and Smith, S.W., 1983. Regional tectonic and earthquake hazard implications of a crustal fault zone in southwestern Washington. J. Geophys. Res., 88: 10,371-10,383.

Figure 1:

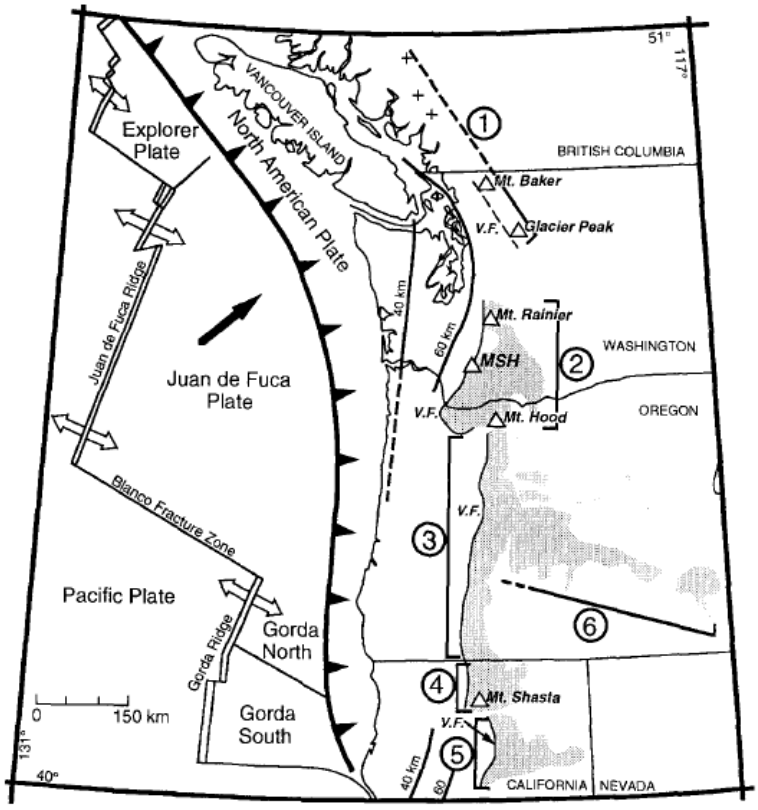

Fig. 1. Map showing volcanic segments (circled numbers and brackets, dashed where uncertain) based on distribution (shaded areas) of vents less than 5 Ma old (Guffanti and Weaver, 1988). Triangles represent selected major Cascade stratovolcanoes; *MSH* = Mount St. Helens. Plate tectonic features of the Juan de Fuca–North American subduction system are from Riddihough (1984). Open arrows show ridge-spreading directions and solid arrow shows direction of convergence between the Juan de Fuca and North American plates. The 40- and 60-km contours (dashed where uncertain) show depth of seismicity in the upper part of the Juan de Fuca and Gorda plates (from Weaver and Baker, 1988). *V.F.* = volcanic front.

Table 1:

TABLE 1

Summary of the eruptive history of Mount St. Helens (MSH)

Eruptive period	Age[a]	Eruptive products
Smith Creek	~4000–3300 a	Dacitic[b] tephras and pyroclastic flows
Pine Creek	~3000–2500 a	Dacitic tephras, pyroclastic flows, domes
Castle Creek	~2200–1700 a	Dacitic tephras and pyroelastic flows Basaltic lavas: I-B[c]: DS-27[d], L82-56 II-B: DS-5, DS-6, DS-7, DS-9 III-BA: L82-63, DS-4, L82-40, L82-41A, DS-78, DS-77, DS-76, DS-74, DS-72, DS-71 Andesitic lavas and tephra: I-A: DS-2, L82-55 II-A: L82-42 TH-A: DS-73, SH-25
Sugar Bowl	800 A.D.	Dacitic tephras, domes
Kalama	1480–~1778 A.D.	Dacitic tephras, pyroelastic flows, lavas and domes; andesitic pyroclastic flows Andesitic lavas and tephra: I-A: SH-3, MSH-484-1, MSH-486-1, DS-79, DS-33, DS-61, L82-57, L82-44, L82-45, L82-47, L82-48 II-A: L82-59
Goat Rocks	1800–1857 A.D.	Dacitic tephra and dome Andesitic lava: II-A: DS-70, MSH-260-1
Current	1980–1986 A.D.	Dacitic tephra, pyroclastic flows, domes

[a]Eruptive periods, ages, and names of eruptive units are from Mullineaux and Crandell (1981), Hoblitt et al. (1980), Crandell (1987), and Hoblitt (1989). Ages for Smith Creek, Pine Creek, and Castle Creek eruptive periods are given in years (=a) before 1992; ages for Sugar Bowl, Kalama, Goat Rocks, and Current eruptive periods are given as dates A.D.

[b]See Smith and Leeman (1987) for detailed information concerning dacitic eruptive products.

[c]See text for definition of groups I-B, II-B, III-BA, I-A, II-A, and TH-A. Appendix 1 gives sample location descriptions and indicates to which stratigraphic units these samples belong.

[d]Sample numbers for all basaltic and andesitic eruptive products included in this study are noted. Sample locations are described in Appendix 1 (except for samples provided by C.A. Hopson and W. Melson for which specific locations were not given).

Figure 2:

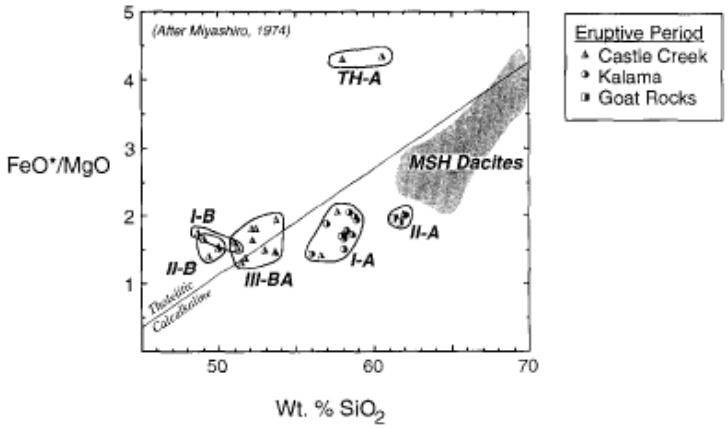

Fig. 2. Classification of MSH eruptive products based on FeO*/MgO and SiO_2. All samples are plotted on this and subsequent major element plots on a 'dry' basis (major elements recalculated to 100%). Samples are plotted according to eruptive period and grouped on the basis of composition (see text for discussion). Shaded field includes data for MSH dacites from Smith and Leeman (1987).

Table 2:

TABLE 2

Major-element compositions (in wt.% oxides) and modal phenocryst abundances for Mount St. Helens mafic to intermediate volcanic rocks

Sample no.:	DS-27	L82-56	DS-5	DS-6	DS-7	DS-9	L82-63	DS-4	L82-40	L82-41A	DS-78	DS-77
Eruptive period:	CC	CC	CC	CC	CC	CC	CC	CC	CC	CC	CC	CC
Rock type:	I-B	I-B	II-B	II-B	II-B	II-B	III-BA	III-BA	III-BA	III-BA	III-BA	III-BA
SiO_2	48.56	50.95	49.28	49.89	49.94	48.92	51.04	51.77	53.08	52.95	52.13	50.99
TiO_2	1.47	1.54	2.00	2.04	1.98	2.10	1.82	1.73	1.6	1.60	1.54	1.56
Al_2O_3	17.47	17.35	16.88	16.82	16.26	16.67	17.06	17.74	16.38	16.43	17.28	17.66
FeO*	11.67	9.54	10.12	10.12	10.53	11.12	8.94	8.53	8.89	8.86	9.65	10.05
MnO	0.16	0.15	0.14	0.15	0.15	0.15	0.14	0.13	0.14	0.15	0.13	0.13
MgO	6.57	6.14	7.16	6.61	6.83	6.67	6.73	6.19	6.07	5.97	5.88	6.17
CaO	9.58	9.33	8.70	8.62	8.54	8.71	8.32	8.30	7.6	7.61	7.93	7.99
Na_2O	3.65	3.60	3.89	3.88	3.90	3.78	3.78	4.24	3.86	3.81	4.03	4.22
K_2O	0.56	0.65	1.26	1.31	1.34	1.36	1.08	1.17	1.04	1.03	1.00	0.97
P_2O_5	0.15	0.20	0.44	0.41	0.38	0.37	0.33	0.20	0.32	0.30	0.29	0.25
Total	99.84	99.45	99.87	99.85	99.85	99.85	99.24	100.00	98.98	98.71	99.86	99.99
Mg #	50.1	53.4	55.8	53.8	53.6	51.7	57.3	56.4	54.9	54.6	52.1	52.3
Modal mineralogy												
GM	87.2	83.5	88.1		80.3	77.3		81.5	89.0	83.5	83.1	83.5
Plag	10.5	11.8	6.0		14.6	15.3		16.1	6.6	11.8	13.4	13.0
Oliv	2.3	4.7	5.9		5.1	7.4		2.3	4.2	4.7	3.5	3.5
Cpx	–	–	tr.		–	tr.		0.1	0.2	–	–	–
Opx	–	–	–		–	–		–	–	–	–	–
Amph	–	–	–		–	–		–	–	–	–	–
Oxides	–	–	–		–	–		–	–	–	–	–

Sample no.	DS-76	DS-74	DS-72	DS-71	DS-2	DS-73	L82-55	L82-42	SH-25	SH-3	MSH-484-1	MSH-486-1
Eruptive period:	CC	CC	CC	CC	CC	CC	CC	CC	CC	Kal	Kal	Kal
Rock type:	III-BA	III-BA	III-BA	III-BA	I-A	TH-A	I-A	II-A	TH-A	I-A	I-A	I-A
SiO_2	52.38	53.65	52.90	52.10	57.63	60.13	56.14	61.52	57.92	58.78	58.26	58.84
TiO_2	1.40	1.30	1.43	1.23	1.14	1.22	1.23	0.85	1.49	1.11	1.22	1.02
Al_2O_3	18.21	18.70	18.31	18.33	17.07	16.85	17.32	17.01	16.63	17.25	16.19	16.74
FeO*	9.40	8.64	8.21	9.52	7.92	8.26	6.89	5.31	9.45	6.82	7.60	7.40
MnO	0.13	0.12	0.13	0.13	0.11	0.11	0.11	0.09	0.12	0.11	0.11	0.10
MgO	5.15	4.46	5.45	5.20	3.83	1.89	4.82	2.62	2.20	3.44	4.28	3.81
CaO	7.70	7.37	7.95	7.99	6.68	5.17	7.12	5.52	5.80	6.24	6.56	6.77
Na_2O	4.27	4.42	4.26	4.25	4.19	4.65	4.14	4.64	4.61	4.52	4.15	4.01
K_2O	1.02	1.04	0.99	0.95	1.12	1.42	1.20	1.43	1.32	1.38	1.29	1.07
P_2O_5	0.20	0.25	0.17	0.25	0.21	0.18	0.21	0.25	0.31	0.26	0.23	0.13
Total	99.86	99.95	99.80	99.95	99.90	99.88	99.18	99.24	99.85	99.91	99.89	99.89
Mg #	49.4	47.9	54.2	49.3	46.3	29.0	55.5	46.8	29.3	47.3	50.1	47.9
Modal mineralogy												
GM	81.5	86.9	80.6	84.7	88.6	84.5	72.1	80.2				
Plag	15.4	12.4	15.5	13.8	9.1	14.1	23.3	16.8				
Oliv	3.1	0.7	3.9	1.5	1.9	–	1.2	–				
Cpx	–	–	–	–	0.4	0.5	0.1	tr.				
Opx	tr.	–	–	–	tr.	0.8	3.3	2.5				
Amph	–	–	–	–	–	–	–	0.5				
Oxides	–	–	–	–	–	0.1	–	–				

Sample no.:	DS-79	DS-33	DS-61	L82-57	L82-59	L82-44	L82-45	L82-47	L82-48	DS-70	MSH-260-1
Eruptive period:	Kal	Kal	Kal	Kal	Kal	Kal	Kal	Kal	Kal	Goat Rx.	Goat Rx.
Rock type:	I-A	I-A	I-A	I-A	II-A	IA	I-A	I-A	I-A	II-A	II-A
SiO_2	56.50	56.94	58.38	57.50	61.63	57.74	58.32	57.91	57.71	61.69	61.40
TiO_2	1.18	0.97	0.91	0.94	0.75	0.95	0.94	1.03	0.93	0.75	0.74
Al_2O_3	17.41	18.16	17.82	17.76	17.51	18.19	17.73	17.56	18.06	18.16	18.50
FeO*	7.56	7.09	7.02	6.58	5.26	6.49	6.41	6.30	6.43	4.80	5.02
MnO	0.11	0.10	0.10	0.11	0.10	0.11	0.11	0.11	0.11	0.09	0.08
MgO	4.24	3.77	3.42	3.92	2.62	3.79	3.71	4.16	3.72	2.51	2.55
CaO	6.88	6.83	6.58	6.74	5.44	6.86	6.64	6.58	6.76	5.89	5.64
Na_2O	4.43	4.58	4.35	4.11	4.53	4.22	4.28	4.45	4.21	4.61	4.70
K_2O	1.24	1.24	1.14	1.15	1.33	1.16	1.19	1.27	1.15	1.27	1.30
P_2O_5	0.35	0.21	0.18	0.16	0.15	0.13	0.19	0.23	0.18	0.16	0.19
Total	99.90	99.89	99.9	98.97	99.32	99.64	99.52	99.60	99.26	99.93	100.12
Mg #	50.0	48.7	46.5	51.5	47.0	51.0	50.8	54.1	50.8	48.2	47.5
Modal mineralogy											
GM	82.3	71.5	61.7	63.0	74.4	59.8		76.8	71.4	78.0	
Plag	16.1	24.3	33.6	30.7	25.3	36.3		19.9	24.7	19.5	
Oliv	0.1	0.6	–	0.4	–	0.4		–	0.3	–	
Cpx	1.1	0.9	2.6	1.5	0.1	1.1		0.3	0.5	0.6	
Opx	0.4	1.6	2.1	3.6	0.2	2.4		3.0	2.9	1.6	
Amph	–	1.1(?)	tr.(?)	0.8(?)	tr.	tr.(?)		tr.(?)	0.2(?)	0.2	
Oxides	–	tr.	–	–	–	–		–	–	0.1	

More than 1000 points were counted per thin section. Phenocrysts of plagioclase (Plag), olivine (Oliv), clinopyroxene (Cpx), amphibole (Amph), orthopyroxene (Opx), and Fe-Ti oxides (Oxides) were defined as > 0.3 mm. Groundmasses (GM) include microphenocrysts (between 0.03 and 0.3 mm). Where the presence of amphibole could only be inferred from pseudomorphs of very fine opaque material, the modal percentage is followed by a (?); tr. = trace amount. Iron oxide is given as total FeO*, and Mg # = 100 × molar $Mg/(Mg+Fe^{2+})$. Samples include products from the Castle Creek (CC), Kalama (Kal), and Goat Rocks eruptive periods.

Table 3:

TABLE 3

Representative microprobe analyses of minerals and anorthite contents of plagioclase in MSH volcanic rocks

Sample no.:	DS-27				DS-9					DS-78		
Rock type:	I-B				II-B					III-BA		
Phase:	OLIV			CPX	PLAG			OLIV		OLIV		
	Ph-C	Ph-R	MP	GM	Ph-C	Ph-R	MP	Ph-C	Ph-R	Ph-C	Ph-R	MP
SiO_2	38.8	38.4	38.7	48.9	51.4	54.2	55.7	38.8	37.5	39.2	37.6	38.4
TiO_2	0.04	0.02	0.04	1.73	–	–	–	0.03	0.05	0.02	0.05	0.06
Al_2O_3	0.03	0.02	0.07	3.01	31.5	29.4	28.1	0.04	–	0.04	0.06	0.16
FeO	21.4	22.6	24.0	13.3	0.54	0.60	0.57	15.0	23.6	17.1	21.5	22.1
MnO	0.34	0.37	0.45	0.28	–	–	–	0.20	0.40	0.22	0.35	0.32
MgO	39.8	39.2	37.8	13.2	–	–	–	44.6	39.1	43.5	39.7	40.0
CaO	0.33	0.32	0.39	19.6	13.9	11.8	10.3	0.22	0.32	0.17	0.21	0.27
Na_2O	–	–	–	0.50	3.23	4.16	4.69	–	–	–	–	–
K_2O	–	–	–	–	0.18	0.32	0.50	–	–	–	–	–
Cr_2O_3	–	–	–	–	–	–	–	–	–	–	–	–
Total	100.74	100.93	101.45	100.52	100.75	100.48	99.86	98.89	100.97	100.25	99.47	101.31
Mg*	76.8	75.6	73.7	63.9	–	–	–	84.1	74.7	81.9	76.7	76.3
Plagioclase:												
Cores:	An_{60}–An_{70}				An_{65}–An_{72}					An_{61}–An_{81}		
Rims:	An_{42}–An_{65}				An_{46}–An_{72}					An_{42}–An_{72}		

Sample no.:	DS-2											
Rock type:	I-A											
Phase:	PLAG				OLIV		OPX			CPX		
	Ph-C	Ph-R	MP-C	MP-R	Ph-C	Ph-R	Ph-C	Ph-R	MP	Ph-C	Ph-R	MP
SiO_2	49.9	58.8	51.8	55.4	29.0	38.0	53.0	53.6	53.1	51.9	52.8	51.7
TiO_2	–	–	–	–	–	0.02	0.18	0.24	0.15	0.54	0.27	0.57
Al_2O_3	31.8	23.0	30.6	26.6	0.02	0.04	1.35	0.91	0.69	3.23	2.58	4.50
FeO	0.53	2.31	0.70	1.75	14.5	26.3	23.9	21.1	22.6	6.02	6.24	5.82
MnO	–	–	–	–	0.16	0.41	0.46	0.48	0.58	–	–	–
MgO	–	–	–	–	44.3	36.7	20.1	20.9	20.4	16.2	17.3	16
CaO	15.0	10.7	13.1	9.90	0.18	0.19	1.12	1.73	2.76	21.3	19.4	19.6
Na_2O	2.77	4.86	3.36	5.08	–	–	–	–	–	0.33	0.42	0.38
K_2O	0.08	0.23	0.14	0.28	–	–	–	–	–	–	–	–
Cr_2O_3	–	–	–	–	–	–	–	–	–	0.44	0.24	0.51
Total	100.08	99.90	99.70	99.01	98.16	101.66	100.11	98.96	100.28	99.96	99.25	99.08
Mg*	–	–	–	–	84.5	71.3	60.0	63.8	61.7	82.7	83.2	83.0
Plagioclase:												
Cores:	An_{61}–An_{75}											
Rims:	An_{49}–An_{69}											

All but plagioclase ranges are given in wt.% oxides. Ranges in plagioclase core and rim composition are given in mole% Anorthite; note that plagioclase compositions for andesitic samples do not include sieve-textured phenocrysts discussed in the text. Symbols: OLIV = olivine, PLAG = plagioclase, OPX = orthopyroxene, CPX = clinopyroxene, AMPH = amphibole, Ph = phenocryst, MP = microphenocryst, GPh = glomerophenocryst grain, GM = groundmass grain, C = core, R = rim, $Mg^* = 100 \times [Mg/(Mg+Fe)]$ (all iron as Fe^{2+}).

TABLE 3 (continued)

Sample no.:	DS-33											
Rock type:	I-A											
Phase:	PLAG					OPX			CPX			
	Ph-C	Ph-R	GM	Ph-C	Ph-R	Ph-C	Ph-C	GPh	Ph-C	Ph-R	Ph-C	Ph-R
SiO_2	55.6	55.7	55.6	57.4	54.1	54.5	53.6	53.9	50.0	49.8	52.5	51.5
TiO_2	–	–	–	–	–	0.19	0.29	0.16	0.31	0.80	0.53	0.61
Al_2O_3	28.0	27.2	28.0	27.2	28.7	0.76	1.42	1.45	3.02	2.82	1.97	2.13
FeO	0.68	0.81	0.93	0.69	0.70	15.7	16.1	16.1	10.8	8.81	8.12	8.39
MnO	–	–	–	–	–	0.20	0.29	0.18	0.25	0.06	0.12	0.05
MgO	–	–	–	–	–	26.9	25.7	26.8	13.6	15.8	15.8	15.4
CaO	11	9.01	10.1	9.27	10.9	1.8	1.78	1.56	20.5	20.4	19	19.8
Na_2O	4.41	5.51	4.96	5.48	4.88	–	–	–	0.39	0.46	0.36	0.43
K_2O	0.23	0.36	0.37	0.36	0.31	–	–	–	–	–	–	–
Cr_2O_3	–	–	–	–	–	–	–	–	–	–	–	–
Total	99.92	98.59	99.96	100.40	99.59	100.05	99.18	100.15	98.87	98.95	98.40	98.31
Mg*	–	–	–	–	–	75.3	74.0	74.8	69.2	76.2	77.6	76.6
Plagioclase:												
Cores:	An_{51}–An_{59}											
Rims:	An_{39}–An_{58}											

Sample no.:	DS-73			DS-70			
Rock type:	TH-A			II-A			
Phase:	CPX	OPX		AMPH	OPX		CPX
	Ph-C	Ph-R	Ph-C	Ph-C	Ph-C	Ph-R	Ph-C
SiO_2	50.5	52.9	53.4	43.2	52.1	52.7	51.5
TiO_2	0.59	0.25	0.30	2.52	0.27	0.27	0.43
Al_2O_3	2.21	1.62	1.32	11.5	1.25	0.72	1.61
FeO	12.6	19.3	21.6	12.9	19.3	20.2	9.46
MnO	0.16	0.22	0.42	0.17	0.52	0.54	0.31
MgO	14.4	23.7	21.3	13.8	25.5	24.7	15.9
CaO	18.8	1.65	2.12	11.3	1.42	1.24	20.3
Na_2O	0.31	–	–	2.27	–	–	0.35
K_2O	–	–	–	0.23	–	–	–
Cr_2O_3	–	–	–	–	–	–	–
Total	99.57	99.64	100.46	97.89	100.36	100.37	99.86
Mg*	67.1	68.6	63.7	65.6	70.2	68.5	75.0
Plagioclase:							
Cores:	An_{52}–An_{63}			An_{52}–An_{65}			
Rims:	An_{49}–An_{55}			An_{46}–An_{58}			

Figure 3:

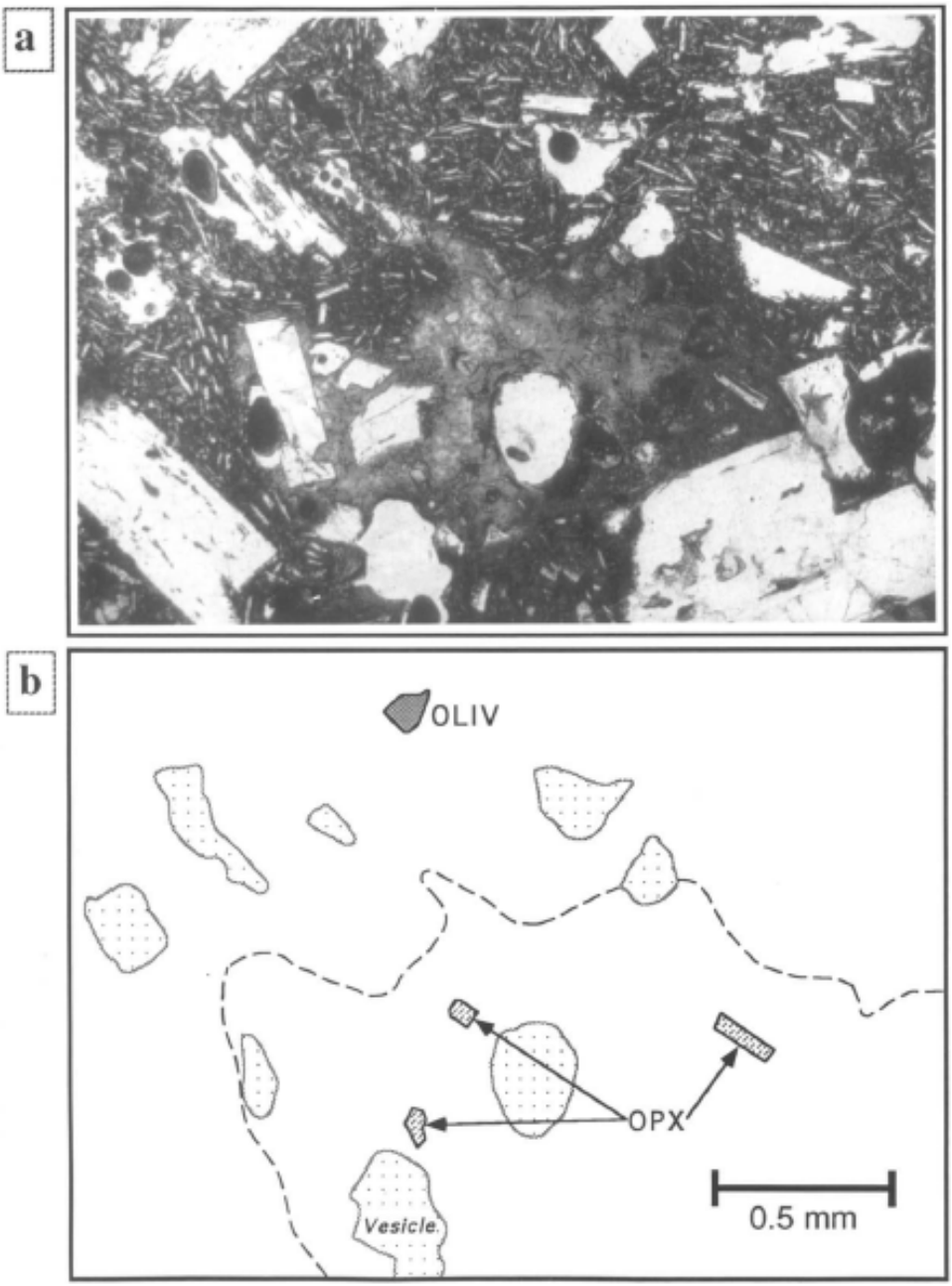

Fig. 3. (a) Photomicrograph of groundmass texture in MSH basaltic andesite (sample DS-4; uncrossed polars). (b) Figure highlighting some features in above photomicrograph (with scale). The dashed line encircles the dacitic "blob" found within a more typical basaltic host. Noted features include orthopyroxene (*OPX*) microphenocrysts within the glassy "blob", an olivine (*OLIV*) microphenocryst within the host, and vesicles (or holes) in the thin section (stippled areas). Plagioclase comprises the other phenocrysts. The diffuse margins of the dacitic blob suggest that it may have been liquid at the time of its incorporation by the host magma. See text for further discussion.

Figure 4:

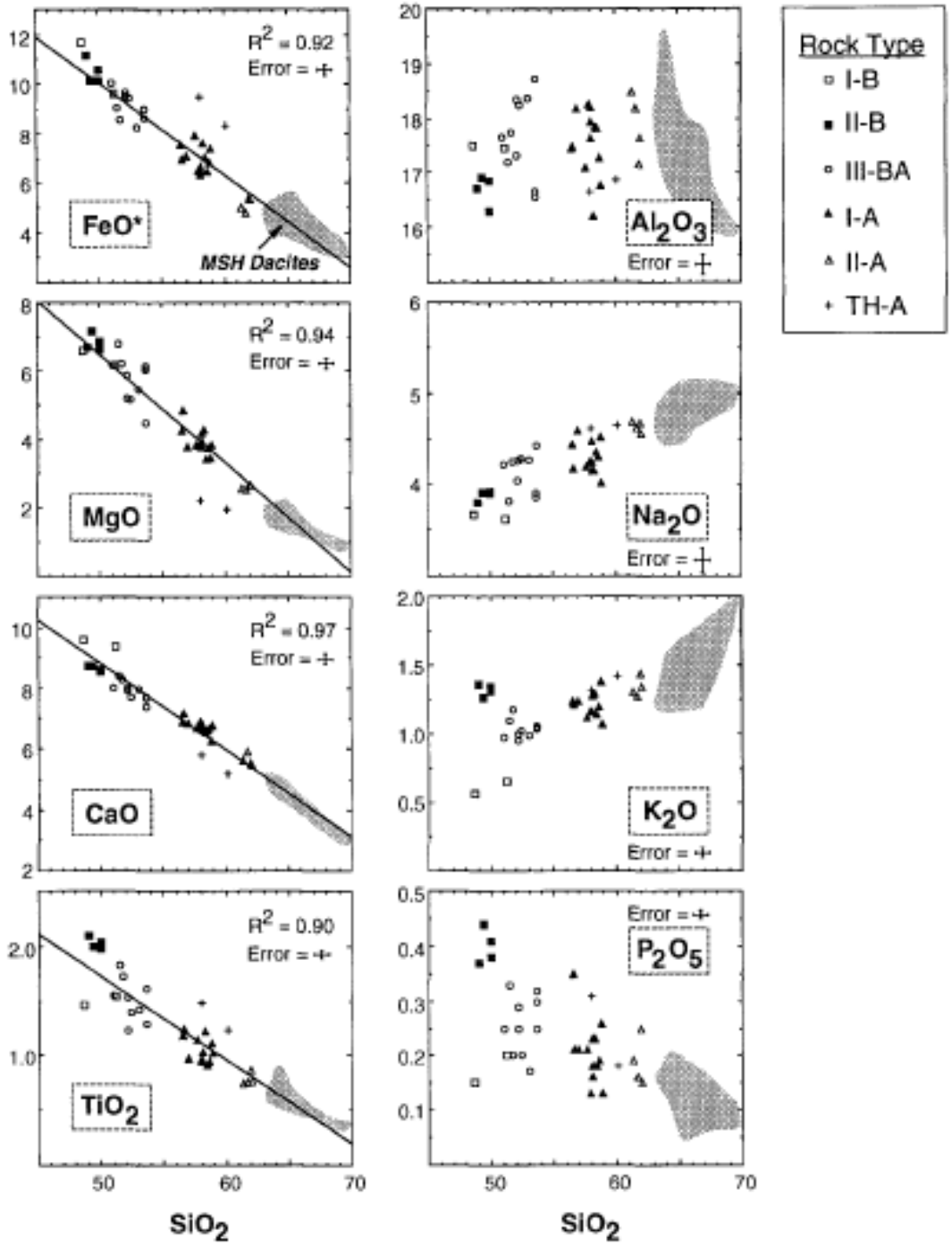

Fig. 4. Major-element (oxide wt.%) Harker variation diagrams for MSH volcanic rocks. Analytical uncertainty for each element is shown by error bars. R^2 denotes the correlation coefficient for linear regressions through data points for FeO*, MgO, CaO, and TiO_2 vs. SiO_2. Shaded field includes data for MSH dacites from Smith and Leeman (1987).

Table 4:

TABLE 4

Trace-element compositions (in ppm) for MSH mafic to intermediate volcanic rocks

Sample no.:	DS-27	L82-56	DS-5	DS-6	DS-7	DS-9	L82-63	DS-4	L82-40	L82-41A	DS-78	DS-77
Eruptive period:	CC	CC	CC	CC	CC	CC	CC	CC	CC	CC	CC	CC
Rock type:	I-B	I-B	II-B	II-B	II-B	II-B	III-BA	III-BA	III-BA	III-BA	III-BA	III-BA
Rb	11	15	27	25	27	24	20	25	22	22	21	–
Cs	0.36	0.38	0.18	0.25	0.60	0.61	–	0.56	–	0.57	0.58	–
Sr	321	363	589	620	577	590	574	581	476	468	514	493
Ba	118	–	272	316	319	312	–	275	–	–	262	221
Y	23.0	27.0	–	24.9	–	26.2	21.0	17.5	28.0	26.0	–	–
Zr	132	139	207	203	203	200	176	188	181	178	178	170
Nb	8.7	11.0	–	32.7	–	28.5	24.0	21.8	18.0	18.0	–	–
Hf	3.0	3.2	4.3	4.3	4.4	4.5	–	4.1	–	4.2	3.9	–
Ta	0.57	0.56	2.30	2.35	2.07	2.13	–	1.41	–	0.95	0.96	–
Sc	33.3	31.0	25.5	25.9	27.3	28.5	–	24.6	–	23.4	23.9	–
V	210		219	212	211	214	–	188	–	–	187	188
Cr	175	140	196	196	157	155	–	169	–	175	152	137
Co	41.7	38.1	35.4	36.3	36.8	38.4	–	32.8	–	33.9	34.4	–
Ni	85	64	86	97	81	84	103	80	107	104	76	72
Zn	83	77	79	74	71	79	78	72	85	89	75	84
La	8.1	10.2	22.7	21.2	19.8	19.8	–	10.8	–	15.6	14.3	–
Ce	21.1	25.0	47.5	45.3	44.2	45.7	–	26.3	–	37.0	34.9	–
Sm	3.51	4.02	5.85	5.53	5.30	5.25	–	3.31	–	4.83	4.43	–
Eu	1.29	1.32	1.85	1.79	1.74	1.80	–	1.36	–	1.53	1.52	–
Tb	0.69	0.77	0.77	0.74	0.73	0.78	–	0.59	–	0.82	0.62	–
Yb	2.35	2.41	2.20	2.11	2.08	2.20	–	1.69	–	2.23	2.10	–
Lu	0.33	0.38	0.31	0.33	0.33	0.30	–	0.25	–	0.34	0.31	–
Th	0.94	1.40	2.60	2.47	2.22	2.26	–	2.05	–	2.10	1.84	–
B	3.4	–	–	4.0	–	5.1	–	–	–	–	–	–
U	–	–	–	–	0.59	–	–	0.61	–	–	–	–
Be	1.0	–	1.8	1.7	1.7	1.6	–	1.6	–	–	1.5	1.5
Pb	5	6	–	5	–	8	8	10	7	10	–	–

Sample no.:	DS-76	DS-74	DS-72	DS-71	DS-2	DS-73	L82-55	L82-42	SH-25	SH-3	MSH-484-1	MSH-486-1
Eruptive period:	CC	CC	CC	CC	CC	CC	CC	CC	CC	Kal	Kal	Kal
Rock type:	III-BA	III-BA	III-BA	III-BA	I-A	TH-A	I-A	II-A	TH-A	I-A	I-A	I-A
Rb	25	25	23	19	32	35	24	27	31	33	29	24
Cs	0.57	0.51	0.31	0.46	1.36	0.94	0.38	0.56	1.15	0.98	0.82	0.68
Sr	527	518	528	511	469	400	594	702	383	523	–	558
Ba	226	244	225	216	334	329	–	–	345	325	310	260
Y	–	–	21.3	–	21.1	23.7	16.0	14.0	–	–	–	–
Zr	165	153	154	156	154	185	162	178	189	153	170	140
Nb	–	–	12.5		10.5	10.2	17.0	12.0	–	–	–	–
Hf	3.6	3.5	3.1	3.6	3.5	4.8	3.7	4.1	4.9	3.7	4.0	3.4
Ta	0.80	0.66	0.67	0.80	0.63	0.74	0.86	0.61	1.00	0.98	1.19	0.47
Sc	21.8	19.0	19.1	21.9	18.1	17.2	19.0	10.5	19.6	15.2	17.7	17.2
V	179	174	184	178	130	112	–	–	153	123	–	139
Cr	99	63	113	98	104	11	96	32	74	103	97	46
Co	32.0	28.5	28.3	32.0	23.6	17.6	25.0	15.6	18.8	19.6	23.6	23.1
Ni	61	57	66	58	46	9	49	21	21	50	–	46
Zn	74	83	74	70	69	81	70	61	75	65	–	66
La	10.9	10.5	11.3	10.0	12.9	12.0	12.4	18.1	17.2	15.9	17.7	9.5
Ce	26.7	24.8	26.8	24.4	29.7	28.4	28.0	39.0	40.2	34.5	39.6	22.7
Sm	3.30	4.17	3.42	3.24	3.65	3.60	3.48	3.98	5.10	3.79	4.22	2.60
Eu	1.30	1.25	1.21	1.26	1.14	1.44	1.25	1.23	1.58	1.20	1.34	1.07
Tb	0.56	0.48	0.49	0.48	0.57	0.63	0.52	0.49	0.82	0.48	0.60	0.38
Yb	1.70	1.68	1.61	1.68	1.75	2.16	1.46	1.23	2.61	1.60	1.68	1.33
Lu	0.24	0.24	0.25	0.25	0.27	0.35	0.23	0.18	0.40	0.23	0.25	0.21
Th	1.66	1.64	1.36	1.54	2.02	2.57	2.40	3.50	2.59	2.26	2.50	2.03
B	–	–	5.7	–	–	14.0	–	–	–	–	–	–
U	0.78	0.94	0.75	0.26	0.87	1.08	–	–	0.82	0.88	0.69	0.60
Be	1.4	1.5	1.5	1.5	1.5	1.8	–	–	1.7	1.5	–	1.0
Pb	–	–	8	–	11	11	8	11	–	–	–	–

TABLE 4 (*continued*)

Sample no.:	DS-79	DS-33	DS-61	L82-57	L82-59	L82-44	L82-45	L82-47	L82-48	DS-70	MSH-260-1
Eruptive period:	Kal	Kal	Kal	Kal	Kal	Kal	Kal	Kal	Kal	GoatRx.	GoatRx.
Rock type:	I-A	I-A	I-A	I-A	II-A	I-A	I-A	I-A	I-A	II-A	II-A
Rb	28	28	24	23	31	22	23	28	23	30	35
Cs	–	0.92	0.84	0.65	–	–	–	0.78	–	1.19	1.25
Sr	595	568	543	553	478	574	542	592	542	484	410
Ba	333	263	292	–	–	–	–	–	–	329	290
Y	19.6	–	15.9	17.0	14.0	16.0	17.0	16.0	16.0	14.8	–
Zr	173	151	147	144	141	145	145	165	140	133	120
Nb	17.5	–	9.0	8.1	7.3	8.1	7.9	13.0	7.9	8.0	–
Hf	–	3.5	3.4	3.1	–	–	–	3.7	–	3.1	3.2
Ta	–	0.59	0.50	0.38	–	–	–	0.67	–	0.44	0.48
Sc	–	16.7	16.4	17.5	–	–	–	16.6	–	12.0	11.5
V	148	152	149	–	–	–	–	–	–	107	–
Cr	92	55	44	29	–	–	–	50	–	39	530
Co	–	22.3	22.0	24.5	–	–	–	23.5	–	15.5	15.2
Ni	40	53	46	37	19	34	35	36	33	18	–
Zn	78	71	74	65	59	67	65	65	68	64	–
La	–	14.7	12.8	12.8	–	–	–	15.1	–	11.6	11.0
Ce	–	30.0	28.7	28.0	–	–	–	33.0	–	25.9	24.8
Sm	–	3.41	3.35	3.47	–	–	–	3.71	–	2.82	2.65
Eu	–	1.15	1.08	0.97	–	–	–	1.20	–	0.96	0.91
Tb	–	0.49	0.47	0.55	–	–	–	0.57	–	0.40	0.35
Yb	–	1.45	1.47	1.57	–	–	–	1.50	–	1.30	1.24
Lu	–	0.22	0.21	0.24	–	–	–	0.22	0.00	0.20	0.19
Th	–	2.34	2.19	2.40	–	–	–	2.80	–	2.14	2.24
B	8.4	–	10.0	–	–	–	–	–	–	–	–
U	–	–	0.72	–	–	–	–	–	–	0.81	–
Be	1.6	1.3	1.4	–	–	–	–	–	–	1.3	–
Pb	13	–	9	11	11	9	12	10	11	11	–

All samples except the L82-series samples were analyzed by D. Smith/W. P. Leeman via ICP (Rice Univ.), INAA (Oregon State Univ.) and XRF (Open Univ.). The L82-series samples were analyzed by G. Fitton (XRF, Univ. of Edinburgh) and M. Norman (INAA, NASA-JSC). Where an element was determined by more than one technique the value given is either (1) a single value obtained by the technique which yielded the highest quality data (as judged by analyses of standard rocks BCR-1, AGV-1, GSP-1, and BHVO-1), or (2) an average of values obtained by multiple techniques where analytical precision and accuracy are comparable.

Figure 5:

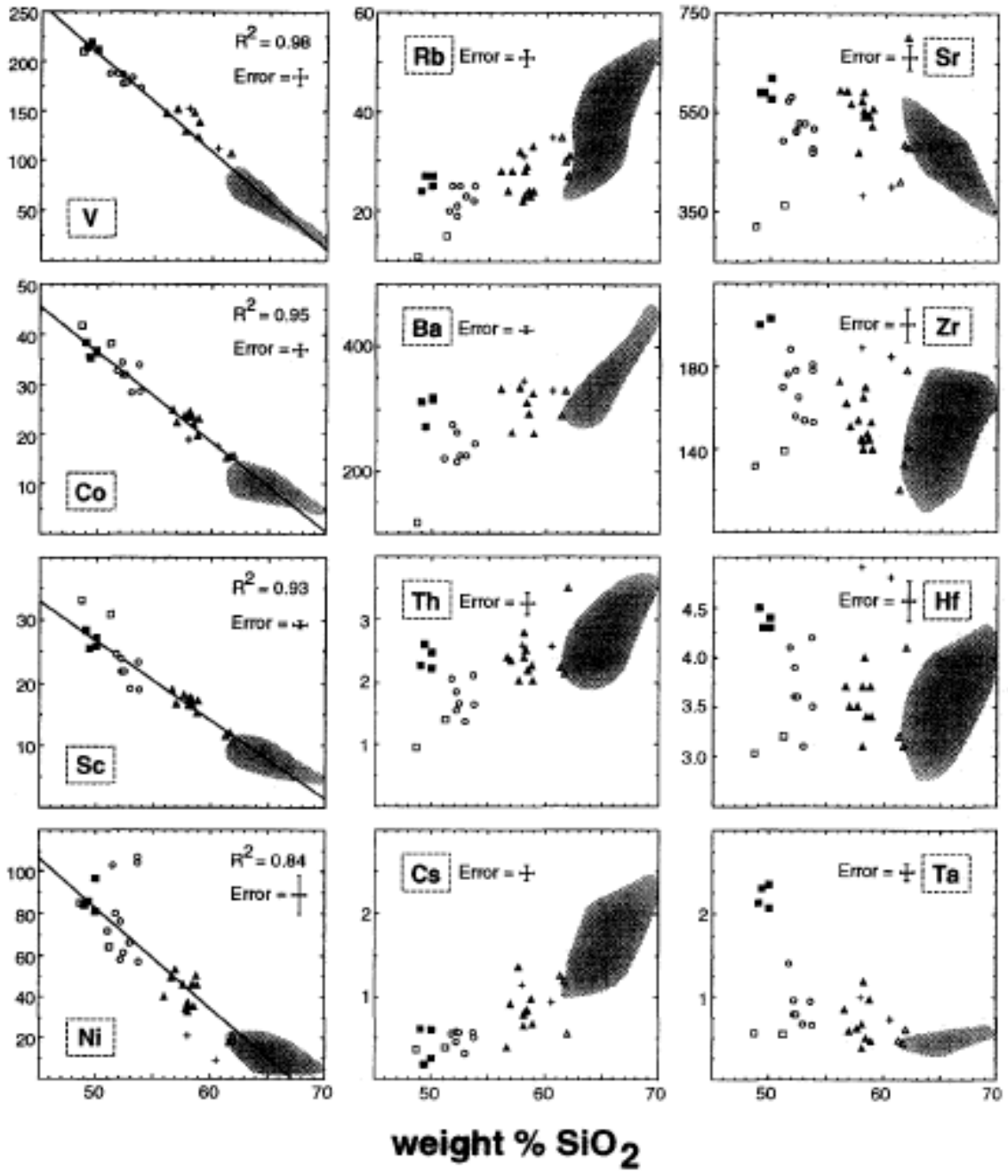

Fig. 5. Trace-element variations (in ppm) in MSH volcanic rocks. Error bars represent estimated analytical uncertainty for each element. R^2 denotes the correlation coefficient for linear regressions through data points for V, Co, Sc, and Ni vs. SiO_2. Symbols and field as in Figure 3.

Figure 6:

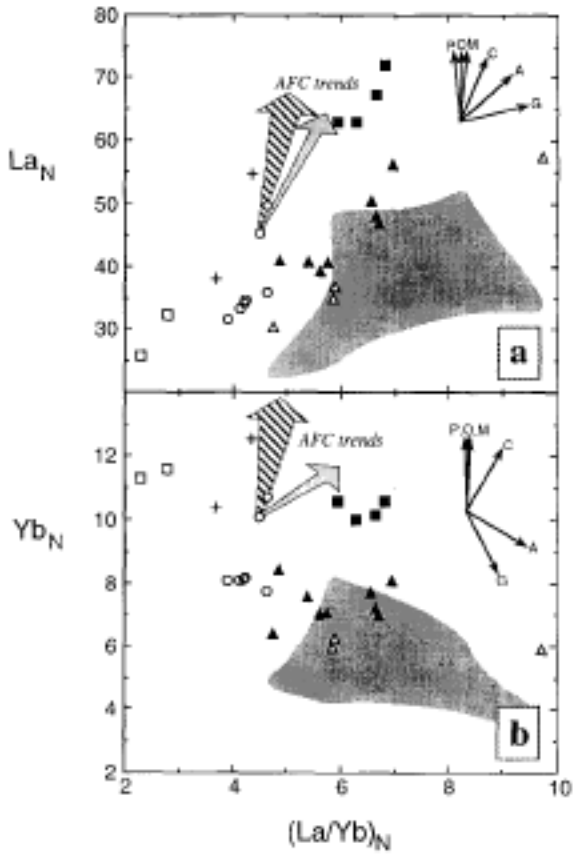

Fig. 6. Chondrite-normalized (a) La and (b) Yb vs. chondrite-normalized (La/Yb) variations in MSH volcanic rocks. Symbols and field as in Figure 3. Vectors are shown for removal of plagioclase (P), olivine (O), magnetite (M), clinopyroxene (C), amphibole (A), and garnet (G). Also shown are representative trends corresponding to assimilation–fractional crystallization (AFC) processes assuming a constant rate of assimilation vs. crystallization ($R_a/R_c=0.5$). The ruled arrows correspond to a crystallization assemblage consisting of 70% plagioclase + 20% olivine + 5% augite + 5% Fe-Ti oxides; the shaded arrows correspond to an assemblage of 45% plagioclase + 10% augite + 40% amphibole + 5% Fe-Ti oxides. Distribution coefficients used to determine mineral vectors and AFC trends are given in Table 5. Assimilants included Tyee sediment (cf. table 8, Smith and Leeman, 1987), upper crust (Taylor and McLennan, 1985), and MSH dacite sample SH-24 (Smith and Leeman, 1987). The size of the AFC arrows encompasses effects of assimilating these various end-members and assume approximately 25% crystallization.

Figure 7:

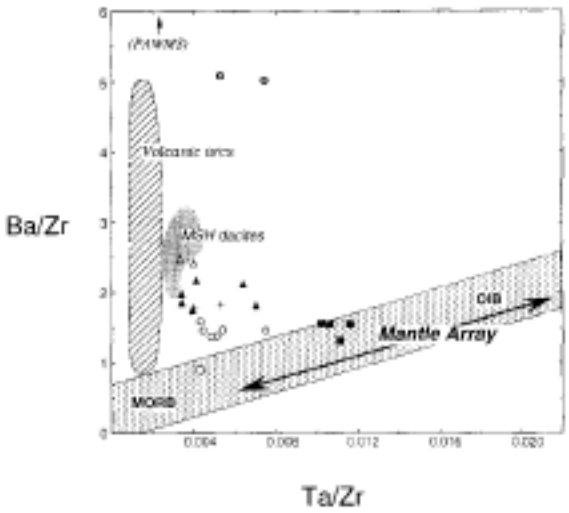

Fig. 7. Ba/Zr vs. Ta/Zr variations in MSH volcanic rocks (symbols and shaded field as in Figure 3). A 'mantle array' (stippled field) defined by typical MORB and OIB is shown for comparison. Note that none of the MSH basaltic rocks (nor most of the dacites) plot within the field for typical volcanic arc magmas (diagonally ruled field; Leeman, unpublished compilation of worldwide results). Values for Tyee sediments (Leeman, unpubl. data) indicated by circled *T*'s. Pacific authigenic weighted mean sediment (PAWMS; Hole et al., 1984) plots off the scale at Ba/Zr = 62.0 and Ta/Zr = 0.0023.

Figure 8:

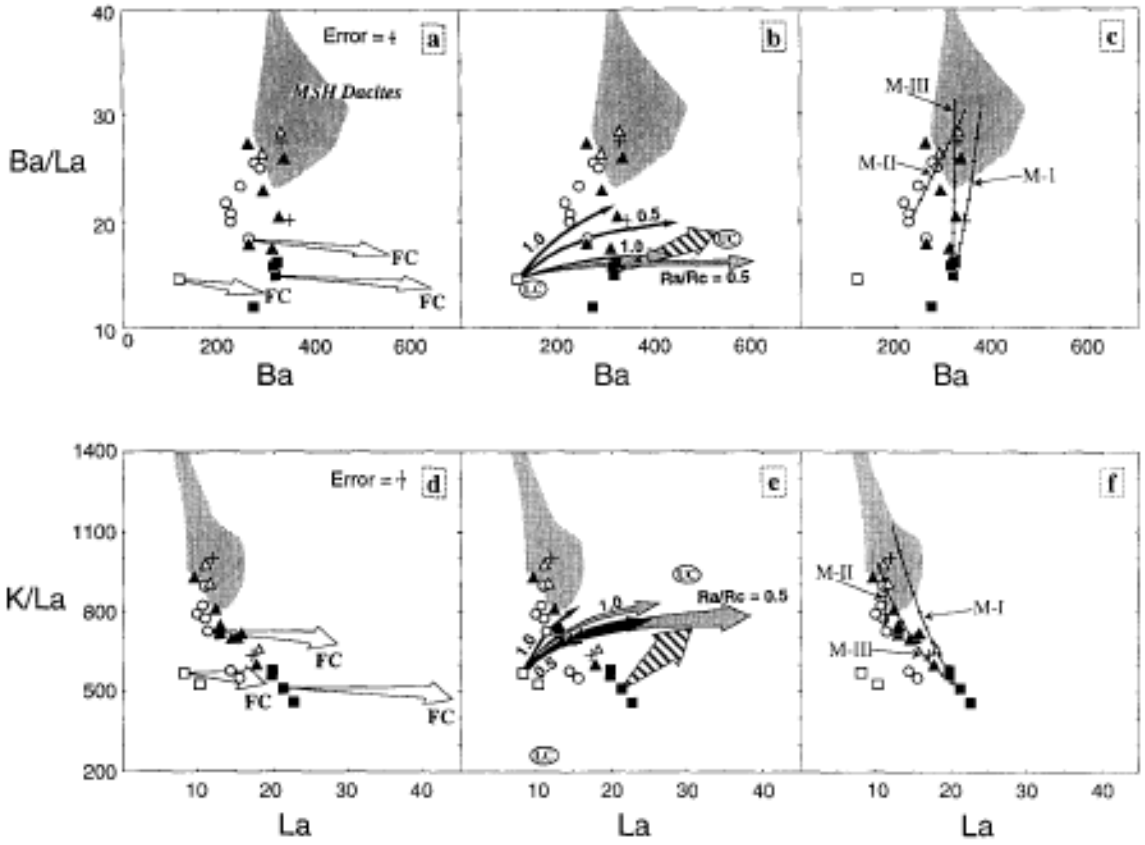

Fig. 8. (a), (b), and (c) Ba/La vs. Ba (ppm), and (d), (e), and (f) K/La vs. La (ppm) variations in MSH volcanic rocks. Symbols and field as in Figure 3. Error bars represent estimated analytical uncertainty for each trace element or ratio. Also shown in (b) and (e) are estimates for upper (*UC*) and lower crust (*LC*) (Taylor and McLennan, 1985). Trends in (a) and (d) labelled *FC* represent closed-system fractional crystallization processes. Trends in (b) and (e) involve assimilation plus fractional crystallization (AFC). Crystallization assemblages and distribution coefficients used in the FC and AFC models are the same as used in AFC models illustrated in Figure 5. The black curves involve assimilation of MSH dacite sample SH-24 (Smith and Leeman, 1987) by type I-B basalt (both erupted during Castle Creek time). The shaded curves involve assimilation of upper crust (Taylor and McLennan, 1985) by type I-B basalt. The ruled curve shows the generalized trend for assimilation of any of the MSH dacites by type II-B basalts. The length of all curves represents approximately equal degrees of evolution via AFC, i.e., 40% crystallization (closed system equivalent), or 20% assimilation (for $R_a/R_c=0.5$) and 40% assimilation (for $R_a/R_c=1.0$; R_a/R_c=rate of assimilation/rate of crystallization). Trends in (c) and (f) represent binary mixing models M-I, M-II, and M-III (see Table 6).

Figure 9:

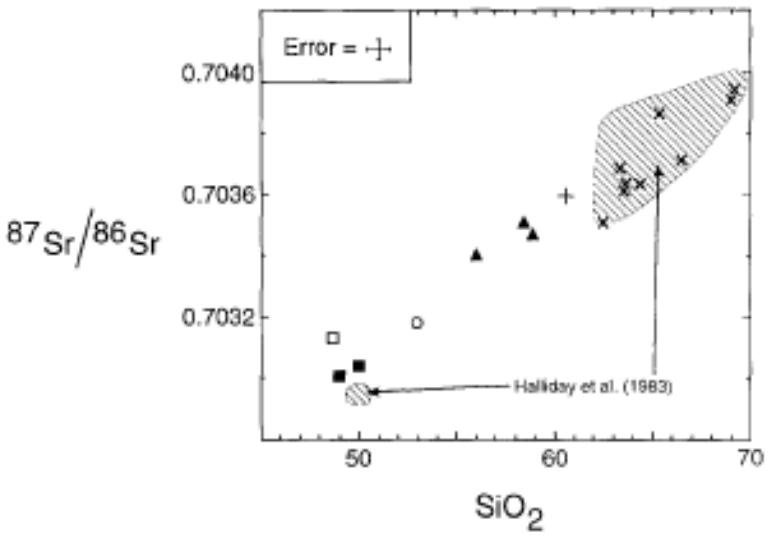

Fig. 9. Strontium isotopic compositions vs. silica in MSH volcanic rocks. Crosses represent MSH dacites (Leeman et al., in prep.); other symbols as in Figure 3. Ruled fields include data for additional MSH samples from Halliday et al. (1983).

Table 5:

TABLE 5

Mineral-melt distribution coefficients used in petrologic models

	Plagioclase	Amphibole	Clinopyroxene	Fe-Ti Oxide	Olivine	Garnet
K	0.17	0.50	0.03	0.01	0.007	–
Rb	0.19	0.33	0.01	0.01	0.006	–
Cs	0.025	0.1	0.01	0.01	0.0004	–
Th	0.01	0.5	0.01	0.28	0.01	–
Ba	0.23	0.4	0.07	0.01	0.006	–
Sr	1.80	0.48	0.14	0.01	0.01	–
Zr	0.02	0.5	0.26	0.25	0.01	–
Hf	0.02	0.5	0.26	0.25	0.01	–
La	0.17	0.25	0.052	0.026	0.002	0.015
Yb	0.038	1.2	0.605	0.089	0.018	4

Sources of values include Shimizu and Kushiro (1975), Pearce and Norry (1979), Henderson (1982), Dostal et al. (1983), and Honjo and Leeman (1987).

Figure 10:

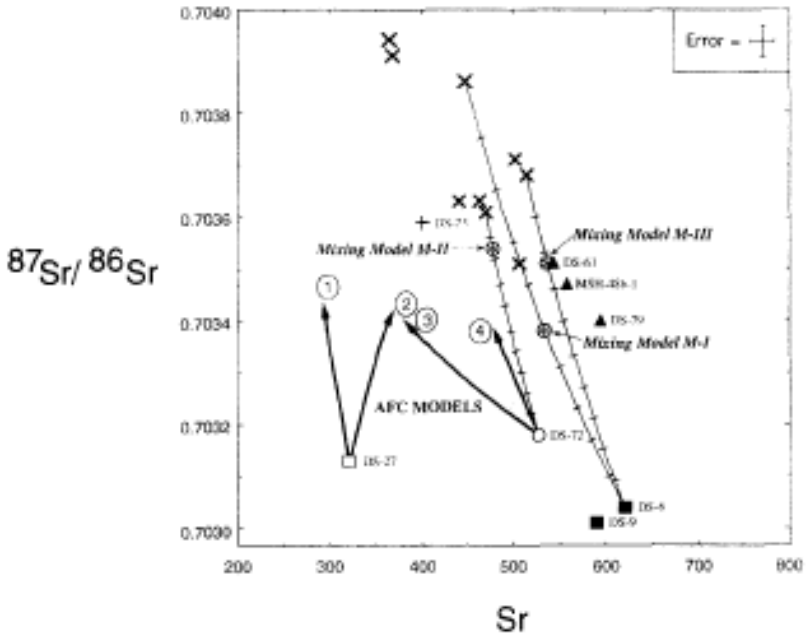

Fig. 10. $^{87}Sr/^{86}Sr$ vs. Sr (ppm) for selected MSH volcanic rocks. Crosses represent MSH dacites; other symbols as in Figure 3. Error bars represent estimated analytical uncertainty for $^{87}Sr/^{86}Sr$ ratios and Sr contents. Curves for four AFC models (1, 2, 3, and 4) are illustrated. The assimilant is a MSH dacite tephra erupted during Castle Creek time (sample SH-24; Smith and Leeman, 1987). Parental magmas include mafic types I-B (DS-27; models 1 and 2) and III-BA (DS-72; models 3 and 4). The fractionating assemblage used in models 1 and 3 is 70% plagioclase + 5% clinopyroxene + 5% Fe-Ti oxides + 20% olivine; the assemblage used in models 2 and 4 is 45% plagioclase + 10% clinopyroxene + 5% Fe-Ti oxide + 40% amphibole. The length of the curves represents the same degrees of AFC evolution as illustrated in Figure 8b,e, i.e., 40% crystallization (closed system equivalent), or 20% assimilation. $R_a/R_c = 0.5$ for the models shown here; models involving R_a/R_c ratios equal to 1.0 have trends within the ranges for the models illustrated, thus they were omitted for clarity. Also shown are curves for mixing between end members used in models M-I, M-II, and M-III (see Table 6); the circled asterisks represent specific andesite compositions calculated in those models.

Table 6:

TABLE 6

Magma mixing models

Model:	M-I				M-II				M-III			
Sample:	DS-6+	SH-18=	SH-3		DS-72+	DS-41=	DS-70		DS-6+	SH-21=	DS-61	
Rock type:	(II-B)	(Dacite)	(I-A)		(III-BA)	(Dacite)	(II-A)		(II-B)	(Dacite)	(I-A)	
Eruptive period:	(CC)	(K)	(K)		(CC)	(GR)	(GR)		(CC)	(PC)	(K)	
% Felsic EM	0.50				0.86				0.77			
	Calculated hybrid	Observed hybrid	Difference	Allowable error	Calculated hybrid	Observed hybrid	Difference	Allowable error	Calculated hybrid	Observed hybrid	Difference	Allowable error
$^{87}Sr/^{86}Sr$	0.70338	n.a.*	–	–	0.70354	n.a.	–	–	0.70351	0.70351	0.00000	0.00006
SiO_2	57.61	58.78	1.17	1.18	61.98	61.69	−0.29	1.23	60.23	58.38	***−1.85***	1.17
TiO_2	1.28	1.11	***−0.17***	0.07	0.71	0.75	0.04	0.05	0.95	0.91	−0.04	0.05
Al_2O_3	17.06	17.25	0.19	0.35	17.82	18.16	0.34	0.36	17.79	17.82	0.03	0.36
FeO*	7.19	6.82	−0.37	0.41	5.44	4.80	***−0.64***	0.29	6.06	7.02	***0.96***	0.42
MnO	0.11	0.11	0.00	0.01	0.10	0.09	−0.01	0.01	0.10	0.10	0.00	0.01
MgO	4.00	3.44	***−0.56***	0.28	2.29	2.51	0.22	0.20	3.01	3.42	***0.41***	0.27
CaO	6.39	6.24	−0.15	0.37	5.41	5.89	***0.48***	0.35	5.89	6.58	***0.69***	0.39
Na_2O	4.49	4.52	0.03	0.27	4.77	4.61	−0.16	0.28	4.44	4.35	−0.09	0.26
K_2O	1.49	1.38	*−0.11*	0.08	1.23	1.27	0.04	0.08	1.23	1.14	***−0.09***	0.07
P_2O_5	0.29	0.26	*−0.03*	0.02	0.16	0.16	0.00	0.01	0.22	0.18	***−0.04***	0.01
Rb	33	33	0.00	5	30	30	0	4	29	24	−5	3
Cs	1.01	0.98	−0.03	0.12	1.05	1.19	0.14	0.14	1.00	0.84	*−0.16*	0.10
Th	2.56	2.26	−0.30	0.32	2.05	2.14	0.09	0.30	2.07	2.19	0.12	0.31
Ba	344	325	−19.00	46	325	329	4	46	320	292	−28	41
Sr	534	523	−11.00	52	478	484	6	48	539	543	4	54
Zr	173	153	***−20.00***	15	133	133	0	13	142	147	5	15
Hf	4	4	−0.20	0.4	3.2	3	0	0.3	3	3	0	0.3
Ta	1.41	0.98	***−0.43***	0.14	0.46	0.44	−0.02	0.06	0.83	0.50	***−0.33***	0.07
Sc	16.2	15.2	*−1.00*	0.9	9.7	12.0	***2.3***	0.7	12.2	16.4	***4.2***	1.0
Co	22.4	19.6	***−2.80***	1.6	14.0	15.5	1.5	1.2	16.7	22.0	***5.3***	1.8
La	16.8	15.9	−0.90	1.0	11.2	11.6	0.4	0.7	12.7	12.8	0.1	0.8
Ce	35.9	34.5	−1.40	2.8	23.8	25.9	2.1	2.1	27.6	28.7	1.1	2.3
Sm	4.08	3.79	−0.29	0.30	2.35	2.82	***0.47***	0.23	3.34	3.35	0.01	0.27
Eu	1.33	1.20	−0.13	0.07	0.90	0.96	0.06	0.06	1.07	1.08	0.01	0.06
Tb	0.57	0.48	*−0.09*	0.07	0.38	0.40	0.02	0.06	0.46	0.47	0.01	0.07
Yb	1.63	1.60	−0.03	0.16	1.25	1.30	0.05	0.13	1.17	1.47	***0.30***	0.15
Lu	0.25	0.23	−0.02	0.02	0.19	0.20	0.01	0.02	0.19	0.21	0.02	0.02
La/Th	6.56	7.04	0.48	1.07	5.46	5.42	−0.04	0.82	6.15	5.84	−0.31	0.89
Ba/La	20.5	20.4	−0.10	3.1	29.0	28.4	−0.6	4.3	25.1	22.8	−2.3	3.5
K/La	738	720	−18.00	60	912	909	−3	76	804	739	*−65*	62
Rb/Th	12.70	14.60	1.90	2.89	14.6	14.02	−0.58	2.78	2.27	1.88	*−0.39*	0.37

SH dacite compositions (SH-21, SH-18, DS-41) used in the models are given in Smith and Leeman (1987); the sample locations are described in Appendix 1. Abbreviations for eruptive periods: CC = Castle Creek, PC = Pine Creek, K = Kalama, GR = Goat Rocks (cf. Table 1). Differences between calculated and observed hybrid compositions which lie outside the range of allowable error are given in bold italics; those which are slightly out of range are given in light italics. The allowable errors given for each model equal two times the absolute analytical error for each element and ratio observed in the modelled andesite.

*n.a. = not available.